A 2.5-kilobase deletion containing a cluster of cine microRNAs in the latency-associated-transcript locus of the pseudorabies virus affects the host response of porcine trigeminal ganglia during established latency

Nada Mahjoub, Sophie Dhorne-Pollet, Walter Fuchs, Marie-Laure M.-L. Endale Ahanda, Elke Lange, Barbara Klupp, Anoop Arya, Jane Loveland, Francois F. Lefèvre, Thomas Mettenleiter, et al.

A 2.5 kb deletion containing a cluster of nine microRNAs in the LAT locus of the pseudorabies virus affects the host response of porcine trigeminal ganglia during established latency.

N. Mahjoub[a,b], S. Dhorne-Pollet[a,b], W. Fuchs[c], M-L. Endale Ahanda[a,b], E. Lange[c], B. Klupp[c], A. Arya[a,b], J. E. Loveland[d], F. Lefevre[e], T. C. Mettenleiter[c], E. Giuffra[a,b,#]

INRA, AgroParisTech, UMR1313 Animal Genetics and Integrative Biology, Jouy-en-Josas, France[a]; CEA, DSV, IRCM, SREIT, LREG, INRA Jouy-en-Josas, France[b]; Friedrich-Loeffler-Institut, Federal Research Institute for Animal Health, Greifswald - Insel Riems, Germany[c]; Computational Genomics, Wellcome Trust Sanger Institute, Wellcome Trust Genome Campus, Hinxton, UK[d]; INRA, Molecular Immunology and Virology Unit, Jouy-en-Josas, France, France[e].

#: Address correspondence to Elisabetta Giuffra, elisabetta.giuffra@jouy.inra.fr

N.M. and S.D-P. contributed equally to this work.

Abstract word count: 249 (250 words limit)

Importance word count: 86 (150 word limit)

Text word count: 6,916 (excluding the references, table footnotes, and figure legends)

Abstract

The alphaherpesvirus Pseudorabies virus (PrV) establishes latency primarily in neurons of trigeminal ganglia when only transcription of the latency-associated transcript (LAT) locus is detected. Eleven microRNAs (miRNAs) cluster within LAT, suggesting a role in establishment and/or maintenance of latency.

We generated a mutant PrV (M) deleted of nine miRNA genes which displayed almost identical properties with the parental PrV (WT) during propagation *in vitro*. Fifteen pigs were experimentally infected with either WT, M or mock infected.

Similar levels of virus excretion and host antibody response were observed in all infected animals. At 62 days post infection trigeminal ganglia were excised and profiled by deep sequencing and RT-qPCR.

Latency was established in all infected animals without evidence of viral reactivation demonstrating that miRNAs are not mandatory for this process. Lower levels of Large Latency Transcript (LLT) were found in ganglia infected by M compared to WT PrV. All PrV miRNAs were expressed, with highest expression found for prv-miR-LLT1, prv-miR-LLT2 (in WT-ganglia) and prv-miR-LLT10 (in both WT and M-ganglia). No evidence of differentially expressed porcine miRNAs was found. Fifty-four porcine genes were differentially expressed between WT, M and control ganglia. Both viruses triggered a strong host immune response, but in M- ganglia gene upregulation was prevalent. Pathway analyses indicated that several biofunctions, including those related to cell-mediated immune response and migration of dendritic cells, were impaired in M- ganglia. These findings are consistent with a function of the LAT locus in the modulation of host response for maintaining a latent state.

Importance

This study provides a thorough reference on the establishment of latency by PrV in its natural host, the pig. Our results corroborate the evidence obtained from the study of several LAT mutants of other alphaherpesviruses encoding miRNAs from their LAT regions. Neither PrV miRNA expression nor high LLT expression levels are essential to achieve latency in trigeminal ganglia. Once latency is established by PrV the only remarkable differences are found in the pattern of host response. This indicates that, LAT functions as an immune evasion locus.

Introduction

Pseudorabies virus (PrV) is a porcine alphaherpesvirus. The genome of PrV is more than 142 kb in size and is characterized by the presence of 70 different coding genes plus the Latency Associated Transcript (LAT) locus (1, 2). PrV is the aetiological agent of Aujeszky's disease causing neurological, respiratory and reproductive disease in the pig, its' natural host. Despite successful vaccination campaigns and eradication of the virus from various countries, Pseudorabies outbreaks still occur in swine populations worldwide, as recently reported in China (3). Because latent infection persists for the lifetime after recovery from acute disease, pigs latently infected by PrV are a constant danger for reactivation and virus shedding and spreading in susceptible populations (4-6).

A particular feature of herpesviruses is their ability to establish and maintain latent infections wherein the virus genome circularizes and persists as an episome. As for other alphaherpesviruses, neurons in the trigeminal ganglia are the primary site of PrV latency (7). Over this period, the transcription of viral lytic genes is repressed and transcription of the viral genome is restricted to the LAT locus overlapping the internal repeat sequence (IRS) (8-10). RNAs of multiple sizes are transcribed from the strand opposite that encoding EP0 and IE180 which can be detected in infected swine trigeminal ganglia (8, 10, 11). The largest is the 8.4-kb Large Latency Transcript (LLT). Transcription from the LAT region is active also during lytic infection of cultured mammalian cells although a different set of transcripts is expressed (12).

MicroRNAs (miRNAs) are small non-coding RNAs approximately 22 nt long that regulate gene expression post-transcriptionally. By complete or partial hybridization, miRNAs induce target mRNA degradation and/or translational repression, and thus serve key roles in the regulation of almost every important cellular process in multicellular eukaryotes (13-15). Given their small size, their lack of antigenicity and their ability to inhibit translation of

specific mRNA species, miRNAs are thought to represent ideal tools for viruses to establish conditions permissive for viral replication, for establishment of latency, or to allow rapid responses to changes in the environment, such as those that trigger reactivation from latency (16-18). The first viral miRNA was identified in Epstein–Barr virus (EBV), a gammaherpesvirus (19). With the advances in sequencing technologies, identification of miRNAs in human and animal herpesviruses rapidly followed (17, 20).

Several alphaherpesvirus have been reported to encode miRNAs which are often clustered in the viral genome, map within the LAT locus or in adjacent regions, and are encoded on both strands (20, 21). In PrV, a cluster of eleven miRNA genes has been identified by deep sequencing in porcine immature dendritic cells (22) and in a porcine kidney (PK15) cell line (23) during lytic infection. This cluster is entirely contained within the ~4.6 kb intron of the large latency transcript (LLT) which functions as a primary miRNA precursor (23).

Here, we report the results of an experimental infection to assess the importance of a miRNA-containing region for the establishment of PrV latency in its natural porcine host. To this end, we generated a PrV clone deleted of a 2.5 kb portion of the LLT intron harboring nine miRNA genes. We adopted a deep sequencing approach to characterize the transcriptional profiles of trigeminal ganglia focusing on miRNAs and coding genes.

Materials and Methods

Construction of virus mutants

The virus generated in this study was derived from the GFP-expressing mutant pPrV-ΔgGG (24), which contains the genome of PrV strain Kaplan (PrV-Ka) (25) cloned as a bacterial artificial chromosome (BAC).

To delete the miRNA cluster, pPrV-ΔgGG (Fig. 1A) was mutagenized in E. coli using the Counter-Selection BAC Modification Kit (Gene Bridges). The provided selection cassette conferring streptomycin sensitivity (RpsL) and kanamycin resistance (KanR) was amplified by PCR (Pfx DNA polymerase, Life technologies) with primers PDMIRN-F (5'-CGGTGGGTCGACGGCTCCTGGGGCTGAAAGCGGCGCTGCGGATCCCCCGCggcctggt gatgatggcgggatcg-3' and PDMIRN-R (5'-GTGTGCGTGTGCGAGAGAGAA GAGATGCGGGGGAGGGCGGCGGGCGCTTGtcagaagaactcgtcaagaaggcg-3'), which contained 5'-extensions (upper case letters) corresponding to nucleotides 98050 to 98099, and the reversal of nucleotides 100571 to 100620 of the PrV-Ka genome sequence, respectively (GenBank accession # JQ809328) (26). The 1419 bp PCR product was used for Red/ET-mediated recombination with pPrV-ΔgGG resulting in pPrV-ΔmiRN (Fig. 1B). Correct insertion of the selection markers, and precise deletion of PrV sequences were confirmed by restriction analyses and Southern blot hybridization, as well as by PCR amplification and sequencing of the mutated genome region (results not shown). Infectious PrV was rescued after transfection (FuGENE HD reagent, Promega) of rabbit kidney (RK13) cells with BAC DNA.

Propagation, titration and growth kinetics of pPrV-ΔgGG and pPrV-ΔmiRN

Rabbit (RK13) and porcine (PK15) kidney cells were used for productive virus replication. RK13 cells were grown in minimum essential medium (MEM) supplemented with 10% fetal bovine serum (FBS). For determination of one-step growth kinetics cells were infected on ice with pPrV-ΔmiRN or pPrV-ΔgGG at a multiplicity of infection (MOI) of 5 and shifted to 37°C after 1 h. After an additional hour, non-penetrated virus was inactivated by low-pH treatment (27) and the inoculum was replaced by fresh medium. At different times of culture at 37°C (Fig. 2), the infected cells were lysed by freeze-thawing, and progeny virus titers were determined by plaque assays overlaid with semi-solid MEM containing 5% FBS

and 6 g/l methylcellulose. Mean titers of three independent experiments, and mean diameters of 30 plaques per virus mutant as well as standard deviations were calculated.

PK15 cells were cultivated in Dulbecco's Modified Eagle's Medium (DMEM) supplemented with 10 % FBS and 100 U/ml Penicillin and 100µg/ml Streptomycin at 37 °C in presence of 5% CO_2. PK15 cells were grown in 6 well culture plates. After reaching 90 to 100% of confluence, cells were infected with either pPrV-ΔgGG or pPrV-ΔmiRN at a MOI of 10 and incubated for 45 min at room temperature. The inoculum was then aspirated, cells were washed several times and incubated with Dulbecco's Modified Eagle's Medium (DMEM) supplemented with 10% FBS. Supernatants and cells were harvested at different times and used respectively i) for viral titrations and growth kinetics as for RK13 cells (Fig. 2), and ii) for total RNA extractions followed by RT-qPCR of viral genes and miRNAs.

Establishment of PrV latency *in vivo*

The *in vivo* animal experiment was approved by an independent ethical committee (7221.3-1. 1-016/12). Fifteen 60 day-old pigs (German Landrace) were used for experimental infection. Animals were housed in the BSL3 facility of the Friedrich-Loeffler-Institut, Germany and tested for absence of PrV antibodies prior to the start of the experiment. Three groups of five animals each were infected intranasally with 10^5 plaque forming units (pfu) of pPrV-ΔgGG (animal no. WT 54-58), pPrV-ΔmiRN (animal no. M 49-53) or mock infected (control group; animal no. C 21-25). The pigs were allowed to recover in the following 62 days to ensure establishment of latency. During this time pigs were monitored for clinical symptoms. In order to check for virus shedding, nasal swabs were collected every two days after infection until virus excretion ceased. Blood samples were collected at 4, 7, 10, 15, 20, 30, 45 and 62 days post infection (p.i.) using a V-trough device.

The host antibody response was assessed by ELISA using PrV gB as antigen. DNA

samples from nasal swabs were analyzed by quantitative Real-Time PCR targeting the gB gene (28).

Animals were slaughtered at 62 days p.i. trigeminal ganglia were excised, rinsed with ice-cold physiological saline solution, frozen in liquid nitrogen within 30 minutes after excision, and stored at -80°C until processed.

Nucleic acid extraction and purification

Total RNAs from infected PK15 cells were extracted using QIAzol Reagent and purified with the RNeasy Mini Kit according to the manufacturer's instructions (Qiagen).

Frozen trigeminal ganglia were homogenized in ice cold TRIzol Reagent using an Ultra-Turrax (IKA-WERK). RNA extraction was performed according to the manufacturer's instructions (Invitrogen). Genomic DNA was obtained upon phase separation for RNA extraction by adding a back extraction buffer containing 4 M guanidine thiocyanate, 50 mM sodium citrate and 1 M Tris pH 8.0 (free base) to the interphase-organic phase mixture. After centrifugation at 12000 x g for 15 min at 4°C, the upper aqueous phase containing DNA was transferred to a clean tube and DNA was precipitated by adding 0.8 volumes of isopropanol per 1 ml of TRIzol, followed by centrifugation at 12000 x g for 5 min at 4°C and pellet washing with 75% ethanol.

Yields and purity of nucleic acids were measured with a NanoDrop ND-1000 spectrophotometer. To remove unwanted residual DNA, all RNA samples were treated with TURBO DNase (Ambion). PK15 RNAs were treated with DNase twice and further checked by qPCR of viral genes to ensure complete removal of PrV genomic DNA. RNA integrity was assessed using an Agilent 2100 Bioanalyzer and RNA 6000 nano kits (Agilent) and the RNA Integrity Number (RIN) (29) was calculated.

Estimation of relative amounts of PrV genomes in trigeminal ganglia

The relative amount of PrV genomes in trigeminal ganglia was estimated by a classical qPCR approach (30). DNA was extracted from a single whole ganglion per animal and amplified using primers specific to the GFP gene (primer forward: GCA AAG ACC CCA ACG AGA AG; primer reverse: TCA CGA ACT CCA GCA GGA CC). For each biological sample, three technical replicates were run and all qPCR were performed on the same run to minimize inter-experimental variation. Triplicate reactions (20 µL) included 5 µL genomic DNA (corresponding to 100 ng of DNA), 10 µL of SYBRGreen PCR master mix and 5 µL of primers (300 nM each). Reactions were incubated in a 96-well optical plate at 95°C for 10 min, followed by 40 cycles at 95°C for 15 s and 60°C for 1 min using a 7900HT Fast Real-Time PCR System instrument (Applied Biosystems). To avoid false-positive results, the DNA of three negative controls was used (samples 22C, 23C and 25C). The PrV genome copy number was estimated per 100 ng of genomic DNA from a PA-GFP-coilin C2 plasmid DNA standard curve.

RNAseq and Small RNAseq libraries preparation and sequencing

Both RNAseq and Small RNAseq libraries were prepared and barcoded using the TruSeq RNA sample preparation kits and protocols of Illumina (www.illumina.com).

RNAseq: libraries were prepared from nine individual samples: three control ganglia, three ganglia latent for pPrV-ΔgGG (WT-ganglia) and three ganglia latent for pPrV-ΔmiRNA (M-ganglia). PolyA-RNA was purified from total RNA using oligo (dT) magnetic beads, fragmented and reverse transcribed using random primers. Libraries were checked with the Agilent High Sensitivity DNA Kit and quantified with the qPCR NGS Library Quantification kit (Agilent). The nine tagged cDNA libraries were pooled, quantitated by qPCR and sequenced in paired-end mode (100 bp reads) on an Illumina HiSeq2000 instrument (TruSeq PE Cluster v3, TruSeq SBS 200 cycles v3 and TruSeq Multiplex Primer kit). Quality control analysis of the raw dataset did not indicate any differences

among lanes regarding the quality or quantity of the reads generated.

Small RNAseq: libraries were prepared for three control ganglia, five ganglia latent for pPrV-ΔgGG (WT-ganglia) and five ganglia latent for pPrV-ΔmiRNA (M-ganglia). Prior to library preparation, integrity of the RNAs was assessed using an Agilent 2100 Bioanalyzer and yields were estimated with a Qubit® Fluorometer. RNAs were fractionated in a 15% denaturing polyacrylamide gel. Small RNA fragments in the range of 18–30 nt were excised from the gel and purified. The 5´ and 3´ termini of the small RNAs were ligated sequentially with adapters, followed by reverse transcription and PCR amplification. The amplified cDNA products pooled were sequenced in single-end mode (50 bp reads) using the TrueSeq SBS kit v3 according to the manufacturer's instruction on a HiSeq1000 Illumina sequencer. Raw reads were analyzed with Casava1.8.2.

The raw reads have been deposited at the European Nucleotide Archive (ENA). RNAseq: accession number PRJEB6754 (http://www.ebi.ac.uk/ena/data/view/PRJEB6754); Small RNAseq: accession number PRJEB6755 (http://www.ebi.ac.uk/ena/data/view/PRJEB6755).

Deep sequencing and differential expression analysis

RNAseq: first, raw 3' ends reads were trimmed for low quality bases. Briefly, the 3' end bases were sequentially cut off if their Phred quality score was below 10 or until the read length became less than 40 bp long. Then, trimmed reads were mapped against the *Sus scrofa* reference genome sequence v10.2 (31) using TopHat v2.0.4 (32). A transcript annotation was downloaded from Ensembl (v.67) (www.ensembl.org) and supplied to TopHat option with "-G". Transcript assembly was performed by providing mapped reads to Cufflinks v2.1.1 (33), option "-g" was used to report all reference transcripts as well as any novel genes and isoforms that were assembled. Transcript quantification was performed using HTSeq-count (from the 'HTSeq' framework, version 0.5.4p3) in default ('union')

mode and these counts were used to perform differential expression analysis. Normalization and a GLM likelihood ratio test were performed using the Bioconductor edgeR package (version 3.2.3) (34) in the R environment (version 3.0.0). Transcripts showing a Benjamin-Hochberg FDR below 0.05 were considered as differentially expressed.

Small RNAseq: first, raw reads were trimmed for adapters and low-quality ends (cutoff Phred quality score: 20) using cutadapt v.1.3 (35). Scripts from the miRDeep2 (v.2.0.0.5) software package (36) were then used for the identification and quantification of novel and known miRNAs from the trimmed reads. Mapping against the pig genome reference sequence (*Sus scrofa v10.2*) was performed with the script mapper.pl while identification of known and novel miRNAs was done using miRDeep2.pl script. The known and predicted miRNAs were then provided to the quantifier.pl script. This module maps the deep sequencing reads to predefined miRNA precursors. These signatures were then post-processed using a custom python script to quantify mature miRNAs. To discard hairpins with a read distribution inconsistent with Drosha and Dicer processing sites (i.e. reads tilled across the precursor), we expected at least a 3:1 ratio between reads that matched on any of the stem-loop arms and reads located in the loop. For the remaining hairpins, reads that mapped inside the loop (more than 3 nucleotides falling in the loop) were not considered for quantification. When no known mature miRNA matched the same precursor, putative new mature miRNAs were named based upon the name of the hairpin on which they were located, or from the name of the known miRNA mapping on the opposite strand of the precursor. All the reference sequences from mature miRNAs and their precursors were obtained from miRBase database, v20 (www.mirbase.org) (37). These counts were used to perform differential expression analysis. Normalization and a GLM likelihood ratio test were performed using the Bioconductor edgeR package (version 3.2.3) (34) in the R environment (version 3.0.0). The miRNAs showing a Benjamin-

Hochberg FDR below 0.05 were considered as differentially expressed.

RT-qPCR analyses

Porcine and viral genes: to validate the RNAseq data of trigeminal ganglia, 16 genes were selected to represent most of the predicted PrV miRNA targets (see below) and a wide abundance range in ganglia (number of RNAseq reads). A second set of genes included the viral genes LLT, EP0, IE180, US1, US3, US7, US8, UL6, UL28, UL32, UL33, UL43, UL47, and UL48. With the exception of primers for LLT, all primers for PrV genes have been reported (38). Primers for LLT and for all porcine genes were designed using Primer3Plus software (39) and verified for specificity by Blast analysis (Suppl. Table 1).

Reverse transcription was performed with the SuperScript III first strand synthesis system (Invitrogen) using between 800 ng and 1 µg of total RNA, and 50 ng of random hexamers. The quantity and quality of cDNAs were evaluated using an Agilent 2100 Bioanalyzer and RNA 6000 pico kits (Agilent). All RT-qPCRs were performed on a 7900HT Fast Real-Time PCR System instrument (Applied Biosystems) using the SYBRGreen PCR master mix. For each primer pair, PCR efficiency was evaluated using serial dilutions of cDNA sample. The potential occurrence of dimers and amplification specificity was assessed by melting curve analyses. An equivalent of 500 pg of cDNA was used as template for each sample and three technical replicates were run as previously described (see “Estimation of relative amounts of PrV genomes in trigeminal ganglia”). A parametric two-tailed Students t-test was used to assess statistical differences between pairwise comparisons.

PrV miRNAs: stem loop RT primers, PCR primers and probes were optimized for improved stability and mismatch discrimination using locked nucleic acid nucleotides (40, 41) (Suppl. Table 1).

Reverse transcription was done using the TaqMan microRNA Reverse Transcription Kit (Applied Biosystems). In each reaction 10 ng of total RNA from trigeminal ganglia/PK15

cells were mixed with 50 nM specific stem-loop RT primer. RT reactions were carried out at 16°C for 30 min, 42°C for 30 min and 85°C for 5 min. The qPCRs were made using standard TaqMan PCR protocols on a 7900HT Fast Real-Time PCR System instrument (Applied Biosystems).

Target gene predictions of PrV miRNAs

The target sites of all PrV miRNAs on differentially expressed genes (Suppl. Table 3) were predicted by TargetScan 6.0 (42, 43). As few genes had annotated 3'UTRs, we first manually annotated as many as possible missing genes making use of cross-species mRNAs where pig specific sequences were unavailable (44). This annotation is available from the Vega website (http://vega.sanger.ac.uk).

Predictions could be computed on 34 out of the 54 differentially expressed genes (Suppl. Table 3). The 3'UTR sequences from EPO (Enredo, Pecan, Ortheus) for 12 eutherian mammal species multiple alignments were retrieved from Ensembl v.68 (www.ensembl.org). Genes having target site context score equal to or greater than zero were filtered out of the analysis. An enrichment analysis was carried out to check if differentially expressed genes were enriched in miRNA targets compared to the number of targets predicted on the total number of genes expressed in ganglia using the Fisher's exact test.

Gene pathway analysis

The Ingenuity Pathways Analysis software IPA (www.ingenuity.com) was used to identify the most relevant biological functions and pathways involving the genes found differentially expressed in pairwise comparisons between WT, M and control ganglia. Firstly we uploaded the list of human homologs that corresponded to the pig genes into the application. The network analysis in the "WT vs. C" and "M vs. C" datasets aimed to search both direct and indirect interactions (known from the literature) between

differentiated genes and all other molecules (genes, gene products or small molecules) contained in the Ingenuity Knowledge Base (IKB). For a given network the degree of association is estimated by considering the proportion of eligible genes (genes with at least one interaction with another full length gene or protein in IKB) and a score is assigned based on the right-tailed Fisher exact test (log(1/p-value). The IPA Upstream Regulator Analysis was used to identify upstream regulators and predict, based on the literature compiled in the IKB, whether they are activated or inhibited, given the observed gene expression changes in the “WT vs. C” and “M vs. C” datasets. The activation z-score predicts the activation state of the upstream regulator, using the gene expression patterns of the genes downstream of an upstream regulator; an absolute z-score of ≥ 2 is considered significant. Finally, the heatmap comparison analysis tool was used to visualize clusters of diseases and biofunctions predicted to increase or decrease similarly across the “WT vs. M” and “M vs. C” datasets. The statistical significance of each biofunction is expressed as p-values from the Fisher’s exact test and a total absolute z-score across all the observations is provided.

Results

Generation and *in vitro* characterization of a PrV miRNA mutant

pPrV-ΔmiRN was generated from the parental pPrV-ΔgGG (Fig. 1A) (24) by deleting nucleotides 98100 to 100570 from the right end of the U_L region of the PrV-Ka genome (Genbank accession no. JQ809328) (26). The deletion includes nine out of the eleven described miRNA genes (22, 23), but excludes the two miRNA genes transcribed from the inverted repeat sequences (prv-miR-LLT10 and prv-miR-LLT11) (Fig. 1B).

The deletion is completely located within the intron of the LLT (8), without affecting the predicted splice donor-, branch-, or acceptor sites. Due to insertion of the bacterial genes

(Fig. 1B) the genome size of pPrV-ΔmiRN is reduced by only 1154 bp compared to pPrV-ΔgGG, which is unlikely to influence significantly the efficiency of viral DNA replication or packaging. Consistently, pPrV-ΔmiRN and pPrV-ΔgGG exhibited almost identical *in vitro* replication properties with respect to replication kinetics and cell-to-cell spread in RK13 and PK15 cells (Fig. 2).

Expression of the genes adjacent the deletion (IE180 and EP0) was profiled by RT-qPCR in PK15 cells. In cells infected with pPrV-ΔmiRN EP0 was transiently overexpressed peaking at 8h p.i. (Fig. 3A and D) while IE180 and the spliced LLT product (exon 1 - exon 2 junction of LLT) displayed very similar profiles of expression in cells infected with either pPrV-ΔmiRN or pPrV-ΔgGG (Fig. 3B and C). Similar expression profiles were found for eleven other PrV genes (not shown). Thus, as desired, mutant and wild-type PrV displayed highly similar *in vitro* properties as an essential prerequisite for the following *in vivo* studies.

Both pPrV-ΔmiRN ("M") and pPrV-ΔgGG ("WT") establish latency *in vivo*

Groups of five animals were infected with pPrV-ΔgGG ("WT"), pPrV-ΔmiRN ("M") or mock infected ("C"). The only clinical symptom detected was intermittent fever until 5 days p.i. All infected animals recovered, while two non-infected control animals died in the course of the experiment due to stress reaction.

The levels of virus excretion in nasal swabs were heterogeneous. On average the animals infected by M showed higher excretion levels than those infected by WT with maximum levels reached earlier (at 2 days p.i.) in two of the M-infected animals. No virus excretion was detected in nasal swabs from 12 days p.i (Fig. 4A, B). All infected animals developed a robust immune response with no differences between M and WT (Fig. 4C, D).

Animals were sacrificed at day 62 p.i. PrV genomes were detected in the trigeminal

ganglia (WT-ganglia and M-ganglia) of all infected animals. Values ranged between 57 and 542 copies per 100 ng of genomic DNA, which is similar to the range found in previous studies on HSV (45). Some of the highest values were found in M- ganglia (Fig. 5). This showed that the deletion did not impair the mutant virus in access to and establishing latency in trigeminal ganglia.

Descriptive statistics of Small RNAseq and RNAseq of trigeminal ganglia

Small RNAseq - We generated individual libraries and profiled by Small RNAseq the ganglia derived from all 13 surviving animals. The sequencing depth ranged from 20.7 to 47.9 million reads with a mean depth of 37.9 million reads per sample. After adapter trimming and filtering out low quality reads, porcine and PrV miRNAs were identified and mapped on the pig and PrV genomes. This led to the identification of between 5.8 and 20.7 million reads per library mapping to known or novel miRNAs (Table 1).

The vast majority of sequences recovered proved, as expected, to be porcine cellular miRNAs. The most highly expressed miRNAs were ssc-miR-27b-3p and ssc-miR-143-3p, with average read counts of about 2 and 1 million respectively. Further analysis did not provide any significant evidence of host miRNAs differentially expressed in the pairwise comparisons among M, WT and C-ganglia. Differences were observed for ssc-miR-204 expression between WT and C-ganglia, and for ssc-miR-429 expression between M and WT-ganglia. However, after manual checking of reads, these turned out to be artifacts due to the abnormally high number of reads in outlier samples, specifically of ssc-miR-204 in one C-ganglia sample and of ssc-miR-429 in one M-ganglion sample (data not shown).

RNAseq - We produced individual libraries for a sub-sample of nine animals (3 M, 3 WT, and 3 C-ganglia). RNAseq profiling generated an average of 65 million reads per library. Quality check confirmed that over 75% of reads were of good quality. Upon mapping and transcript assembly, we detected 19,465 pig genes expressed in ganglia. Normalized

values are provided in Suppl. Table 2. The most expressed pig genes (average of 700,000 reads per sample) corresponded to the neurofilament medium and light polypeptide genes (NEFM and NEFL), which are found highly expressed in the cerebral cortex and in the hippocampus (46, 47). Despite the depth of sequencing, very few reads mapped on the PrV genome (between 51 and 523 normalized reads). All of them mapped to the LLT gene locus as expected during latency (Suppl. Table 2).

All the known PrV miRNAs are expressed during latency

In the ganglia latent for parental PrV (WT-ganglia), we detected all the mature PrV miRNAs described so far, which are encoded by 11 miRNA genes clustering in the LLT intron (22, 23). No new PrV miRNAs were identified (Table 2). Furthermore, we did not detect the offset-moRNA encoded by the prv-mir-LLT8 gene previously found in dendritic cells during productive PrV infection, identified as prv-miR-4 by (22) and as moR-8 (23, 48).

The PrV miRNAs are still annotated as unique mature sequence in the last version (v21) of the miRBase database (www.mirbase.org). However, with few exceptions, all miRNAs were found expressed by both the 5p and 3p arms of their precursor sequence, and, as expected, one form was predominant (Table 2). Furthermore, the predominant mature miRNAs encoded by the prv-mir-LLT7 and prv-mir-LLT8 genes were those of the 3p arm as previously detected (23, 48) but not yet annotated in miRBase. To clarify the issue, we revised the nomenclature of all PrV miRNAs by adding the arm of origin information (Table 2).

The most abundant viral miRNA was prv-miR-LLT2-5p followed by prv-miR-LLT1-3p (both deleted in M), and prv-miR-LLT-10-3p (present in both WT and M) (Table 2). The prv-mir-LLT-10a and prv-miR-LLT-11a genes map to the 3’ distal portion of the LLT intron and are duplicated in the terminal repeat region (TR) of the PrV genome (prv-mir-LLT10b and prv-

mir-LLT11b). The mature prv-miR-LLT-10 and prv-miR-LLT-11 showed similar patterns of expression in M and WT- ganglia, suggesting that the deletion in the mutant virus did not affect regulatory sequences required for the expression of prv-mir-LLT10a and prv-mir-LLT11a (Table 2).

The RT-qPCRs confirmed the presence of the three most abundant miRNAs (prv-miR-LLT1-3p, prv-miR-LLT2-5p and prv-miR-LLT-10-3p) (Fig. 6A). For comparison, we checked the expression of these miRNAs in PK15 cells during productive infection at 12h p.i. Both prv-miR-LLT1-3p and prv-miR-LLT2-5p were highly expressed while prv-miR-LLT-10-3p was detected at much lower levels (Fig. 6B). We were unable to assess the expression levels of other less abundant PrV miRNAs above background values.

Characterization of the pattern of expression of the LAT locus in trigeminal ganglia

RNAseq and Small RNAseq data indicated that only LLT and the viral miRNAs (which, with the exception of prv-miR-LLT10 and prv-miR-LLT11, are only present in the genome of WT) were expressed in the porcine ganglia, as it would be expected in established latency. To better characterize this status in the M-ganglia we performed RT-PCR and RT-qPCR analyses of different portions of the LAT locus adjacent to the deletion (Fig. 1).

In both M and WT-ganglia no expression of IE180 or EP0 could be detected by repeated tests by primer-specific RT-qPCR. This confirmed that also the second copy of the IE180 gene mapping to the TR region of the PrV genome (1) is inactive during latency. The M virus expressed lower levels of transcripts comprising the ex1/ex2 junction and exon 2 of LLT, while the first LLT exon was expressed at similar levels by both viruses (Fig. 7). This was surprising, given that the splicing of LLT (LLT ex1/ex2 junction) was unaffected *in vitro* (Fig. 2C) and no expression of genes expressed during the lytic phase was detected in ganglia.

An additional difference was observed in the distribution of RNAseq reads between M and WT-ganglia at the LAT locus. This revealed that in M-ganglia the portion of the LLT intron ~ 1000 bp immediately downstream the deletion is expressed (Fig. 8). We tested by RT-qPCR if this could indicate the presence in M-ganglia of unspliced transcripts which are expressed during the PrV lytic phase (12). The results confirmed that the bacterial genes and the LLT intron region immediately downstream of the bacterial cassette (Fig. 1) were expressed by the M virus, indicating that the bacterial promoter is active in ganglia. However, in agreement with the distribution of mapped reads, no expression of the portion of the LLT intron adjacent to the acceptor site and preceding the peak of reads at the 5' of LLT exon 2 was detected by RT-qPCR in M and WT-ganglia (not shown). This excluded the possibility that transcripts covering part of the 3' portion of the intron are expressed in M-ganglia.

Gene upregulation is prevalent in trigeminal ganglia latent for the mutant PrV

By differential expression analysis of the nine samples profiled by RNAseq, we identified 54 genes (plus two pseudogenes and two miRNA precursors predicted in the cow genome), each significantly differentially expressed (DE) in at least one of three pair-wise comparisons among WT, M and C- ganglia (WT vs. C, M vs. C and M vs. WT). Values of differential expression (DE and p-values of significance) are provided in Suppl. Table 3.

M-ganglia and WT-ganglia differed considerably in their patterns of gene expression. DE genes reaching significance were more abundant in WT- (34) than in M-ganglia (22), and only eight genes were common to the M vs. C and WT vs. C comparison. An additional six genes were significantly DE only in the direct comparison between WT vs. M.

Remarkably, while in the WT-ganglia we found a prevalence of significantly downregulated genes (20 downregulated vs. 14 upregulated), the opposite trend was found in M-ganglia (19 upregulated vs. only 3 downregulated) (Suppl. table 3). Only BTNL9 (butyrophilin-like

9), MTNR1B (melatonin receptor 1B), NR1D2 (nuclear receptor subfamily 1, group D, member 2, which is a transcriptional repressor with roles in circadian rhythms and carbohydrate and lipid metabolism) and MAPK4 (Mitogen-activated protein kinase 4) were more significantly downregulated in M-ganglia in comparison to WT-ganglia or controls.

The eight genes shared by the M vs. C and WT vs. C comparisons included only highly upregulated host immune genes: CXCL13 (a chemokine ligand); five immunoglobulins (IGJ, Igk-V, IGKV-6, one IGLC member and IGLL5); TNFRSF10B (member 10B of the TNF-receptor superfamily, the most upregulated gene found in both M and WT-ganglia (> 4 logFC); and a protein annotated as novel in the pig genome similar to SLC2A7, which is a glucose transporter (Suppl. Table 3).

The RT-qPCR of 16 genes represented by either a high or low number of RNAseq reads was carried out in the whole set of WT, M and C-ganglia samples. The results showed excellent concordance between RNAseq and RT-qPCR. Furthermore, the profile of these few additional animals provided significance to previously suggestive values (Table 3, Suppl. Table 3). In particular, PLA2G2D (Phospholipase A2, group IID), CD8A (T-cell surface glycoprotein CD8 alpha chain) and CXCL9 became significant also in the M vs. WT contrast, strengthening the pattern of gene upregulation found in M-ganglia. Furthermore, RT-qPCR confirmed that VIP (vasointestinal peptide) was detectable only in the three M-ganglia samples carrying the highest numbers of copies of PrV genomes (Fig. 5).

Fifteen DE genes harbored one or multiple targets for one or more of PrV's miRNAs (Suppl. Table 3). However, the generalized pattern of gene downregulation in WT-ganglia and of gene upregulation in M-ganglia hid any putative modulatory effect of PrV miRNAs. Furthermore, we did not detect any relative enrichment of putative targets for the most expressed PrV miRNAs compared to the whole set of porcine genes expressed in ganglia

(not shown).

The LAT deletion affects the host pro-inflammatory response

We used the Ingenuity Pathway Analysis (IPA) software (www.ingenuity.com) to analyze the expression patterns of latently infected ganglia. All the genes which were DE in at least one of the three comparisons (Suppl. Table 3) were included in the analysis, with the exception of the two putative miRNA precursors so far annotated only in the cow genome (bta-mir-2887 and bta-miR-2904) and C3 (missing in the IPA reference database). By this analysis we could assign a total of 44 these DE genes to top gene networks and/or biofunctions.

The top network identified by IPA in both M- and WT-ganglia was “Cell-mediated Immune Response, Cellular Movement, Hematological System Development and Function” (17 genes; score 39), followed by “Hereditary Disorder, Neurological Disease, Psychological Disorders” (15 genes; score 34) (Suppl. Table 4). Other networks were identified by less than six genes in either the WT vs. C or M vs. C comparisons.

IPA identified INFG and two inflammatory cytokines (TNF and IL6) as most significant top upstream regulators. The state of activation of these regulators was globally coherent with the pattern of expression of 20 DE genes in the WT vs. C and M vs. C comparisons (Fig. 9). As expected, the large majority (15) of these genes belonged to the cell-mediated immune response network (Suppl. Table 4). This network added evidence for the pattern of expression of VIP being inconsistent with the activation of TNF while the pattern of CYP2E1 (cytochrome P450, family 2, subfamily E, polypeptide 1) is inconsistent with all the three regulators (Fig.9).

In order to compare the WT and M-ganglia for their respective status of activation of specific diseases and biofunctions, we generated a comparative heatmap of M vs. WT-

ganglia reporting the IPA z-scores of activation besides the p-values of biofunctions' significance (Table 3). The differences in the trend of activation/inhibition between WT- and M-ganglia are largely determined by few genes participating to several biofunctions. The "migration of dendritic cells" was, together with the more general ones related to tissue and cell homeostasis, the most significant biofunction of latent ganglia (p-value: $6.77E^{-06}$). Differently than in WT-ganglia, in M-ganglia this biofunction had a trend of inhibition. This difference was due to the combined effect of three genes: VIP (only expressed in M-ganglia); AGT (angiotensinogen - serpin peptidase inhibitor, clade A, member 8; less downregulated in M-ganglia) and ICOS (inducible T-cell co-stimulator; more upregulated in M-ganglia). A similar effect was found for other biofunctions ("activation of leukocytes", "activation of T lymphocytes", and "inflammatory response"). Conversely, "expansion of T lymphocytes" and "stimulation of cells" had a trend of activation in M-ganglia due to the combined effect of VIP and BTNL9 (the latter more downregulated in M-ganglia). Interestingly, M-ganglia showed also a less efficient inhibition of "synthesis of fatty acid" and "concentration of fatty acid" (Table 3).

Discussion

We show here that deletion of nine of the eleven known PrV miRNA genes, contained in a cluster within the LLT intron sequence, does not impair establishment of latency in trigeminal ganglia. The PrV genome was detected in the trigeminal ganglia of all infected animals beyond the termination of clinical symptoms and viral excretion (Fig. 4, Fig. 5). Moreover, the mutant virus displayed almost identical properties with the parental pPrV-ΔgGG, a BAC clone derived from PrV-Ka, during propagation *in vitro* (Fig. 1, Fig. 2, Fig. 3).

The value of our experimental approach lies in the use of a natural virus-host system to analyze the importance of miRNA-containing regions on herpesvirus latency. Most of the

current knowledge on latency has been obtained from studies of HSV-1 and HSV-2 in rodent models. In these settings, all LAT mutants that ablate LAT expression and, thus, the expression of multiple miRNAs, can establish and maintain latency (18, 41-43). It has been reported earlier that PrV mutants unable to express LAT and EP0 were also able to reach and persist in porcine trigeminal ganglia after intranasal infection (49). This makes it unlikely that removal of the entire cluster of eleven PrV miRNA genes would make a difference for the ability of PrV to establish latency.

Transcriptional patterns of the PrV genome during latency

With the exception of the deleted miRNAs, the viral transcriptional profiles of ganglia latent for the mutant “M” PrV displayed only subtle differences compared to the parental “WT” virus. The finding that the levels of ex1/ex2 junction and exon 2 of LLT were decreased in M-ganglia (Fig. 7) is difficult to explain in absence of any evidence of viral reactivation. In HSV several results point to products of the LAT locus functioning in repression of lytic gene expression, which would favor establishment and maintenance of latency, and LAT has been proposed to silence viral gene expression as a long non-coding RNA (50-52). However, in HSV the number of neurons harboring virus is decreased after infection by ΔLAT mutants, as reviewed by (53), while ganglia latent for the mutant PrV (M-ganglia) carried similar amounts of latent PrV genomes compared to WT-ganglia (Fig. 5). Decreased levels of LLT in ganglia latent for the nine miRNA-deleted virus are also inconsistent with the predicted ability of multiple PrV miRNAs to target LLT, as well as IE180 and EP0 (23). Finally, given the limited knowledge of the PrV LAT locus, we cannot totally exclude that the 2.5 kb deletion removed regulatory sequences which may affect LLT expression in neurons (54).

In addition to LLT, all the PrV miRNAs previously described from productively infected cells (22, 23) were detected in latent ganglia (Table 2, Fig. 6). The two most abundant miRNAs

552 in WT-ganglia prv-miR-LLT1-3p, prv-miR-LLT2-5p, which are absent from the mutant PrV
553 genome, are highly expressed during productive infection in PK15 cells (Table 2, Fig. 6).
554 Prv-miR-LLT1 is also the most highly expressed PrV miRNA in dendritic cells (22) and is
555 the only one detected in trigeminal ganglia of pigs during acute infection, albeit at reduced
556 sequencing depth (48). It is interesting that prv-miR-LLT10-3p, which is not included in the
557 deletion, was expressed by both M and WT at similar levels as prv-miR-LLT1-3p and prv-
558 miR-LLT2-5p, which contrasts with the low expression of this miRNA during productive
559 infection (Table 2, Fig. 6). It should be noted that the gene coding for this miRNA is
560 duplicated, and maps at the 3' end of both copies of IE180 (1). The fact that IE180
561 expression was not detected suggests that the mature prv-miR-LLT10 is expressed only
562 by the miRNA gene copy adjacent to the LAT locus.

563 These findings suggest that, as for HSV (55), different PrV miRNAs may be expressed
564 preferentially during productive infection in cell culture and during latent infection in
565 sensory ganglia. In this context, it is interesting that the only difference found was a
566 transient upregulation of EP0 at 8h pi (Fig.3A and D) in PK15 cells infected by the mutant
567 virus. Otherwise, the absence of miRNAs did not affect the replication properties of PrV
568 (Fig. 2).

569 **Transcriptional patterns of the host genome during latency**

570 Our findings add to what had been proposed for HSV, i.e. that host parameters such as
571 innate immunity (56), the repressive effects of immune cells in ganglia (57), or the
572 neuronal environment (58) promote the establishment and maintenance of latency (52).
573 Host genes which are differentially expressed during PrV latency are involved in
574 biofunctions related to expansion, activation and cell death of T lymphocytes and of
575 dendritic cell migration. This parallels data from HSV latency, where the LAT locus has
576 been shown to function as an "immune evasion gene" by promoting functional exhaustion

of virus-specific CD8+ T cells in latently infected trigeminal ganglia and by inhibiting the phenotypic and functional maturation of dendritic cells (59, 60).

Indeed, the most prominent differences between ganglia latent for the miRNA-deleted (M) and parental (WT) PrV were found in host response, and, interestingly, without any evidence for differential expression of host miRNAs. Both viruses triggered a robust pro-inflammatory immune response (Suppl. Table 4, Fig. 9) but a pronounced pattern of gene upregulation was found in ganglia latent for the mutant virus (Suppl. Table 3, Table 3). The impairment of the host pro-inflammatory response is reflected by differential expression of a limited number of genes acting in several pathways (Table 4). VIP acts as an inhibitor in many biological functions. Its absence induces better Th1 polarization and antiviral immunity in mice (61) and VIP-knockout mice have enhanced cellular immune responses and increased survival following murine cytomegalovirus infection (62). Various reports indicate CYP2E1 (as a gene downregulated by various stimuli, including inflammation (63). Thus, in M-ganglia VIP would be a factor of less efficient cell mediated host response, and the upregulation of CYP2E1 would be a global indicator of reduced inflammatory response (Table 3, Figure 9). Conversely, reduced levels of BTNL9 suggest a reduced ability of the mutant virus to control T cell activation (Table 3). The butyrophilin-like family encodes transmembrane glycoproteins with roles in immune co-regulation and antigen presentation, and some of them are functionally implicated in T cell inhibition and in the modulation of epithelial cell-T cell interactions (64-66).

The pattern of gene upregulation found in the ganglia latent for the mutant virus is suggestive of a role for PrV miRNAs in regulating the host genome during latency. However, presumably only a fraction of the observed effects can be attributed to PrV miRNAs. Other regulatory sequences controlling the latent virus genome at the epigenetic level (54, 67) may map to the 2.5 kb region deleted from the PrV LAT locus and alter host transcription and immune responses. Additional functional studies are required to

603 investigate the relative contribution of these different factors during PrV latency.

604

605 **Acknowledgments**

606 We would like to thank Laura Duciel for the technical assistance, Nicolas Pollet for
607 providing the PA-GFP-coilin C2 plasmid DNA, Florence Jaffrezic and Andrea Rau for help
608 in statistical analysis, Jordi Estellé for help in setting up the RNAseq analysis pipeline,
609 Electra Tapanari for help with the 5' and 3' end gene data, and Maria Bernard for help in
610 the database submission of sequencing datasets. This work has benefited from the
611 facilities and expertise of the IMAGIF platform (Centre de Recherche de Gif -
612 https://www.imagif.cnrs.fr) and of the Genome and Transcriptome core facilities of the
613 GenoToul platform (http://get.genotoul.fr). The research leading to these results has
614 received funding from the European Community's Seventh Framework Programme
615 (FP7, 2007-2013), Research Infrastructures action, under the grant agreement No. FP7-
616 228394 (NADIR project), and by the "INRA Package" grant (2011-2014) of EG.

617

618 **Figure legends**

619 Figure 1

620 (A) Physical map of the PrV-Ka genome containing unique (U_L, U_S) and inverted repeat
621 (IR, TR) sequences. BamHI restriction sites and fragments, as well as the insertion of a
622 bacterial vector and of an EGFP reporter gene cassette at the gG gene locus in pPrV-
623 ΔgGG (Fuchs et al., 2012) are indicated. (B) An enlarged section shows the boundary
624 between U_L and I_R with the open reading frames of the regulatory proteins EP0 and IE180.
625 Viral mRNAs and the spliced large latency transcript (LLT) are indicated by dotted arrows.
626 Identified miRNAs (Wu et al., 2012) are shown as red arrowheads numbered from 1 to 11

627 (corresponding to miRNA genes: from prv-mir-LLT1 to prv-mir-LLT11). In pPrV-ΔmiRN the
628 majority of the miRNA genes was deleted and replaced by selection markers (RpsL, KanR)
629 used for BAC mutagenesis in *E. coli*.

630 Figure 2

631 Replication of pPrV-ΔgGG and pPrV-ΔmiRN in PK15 (A) and RK13 (B) cells. Progeny virus
632 titers were determined between 4 and 24h after infection at multiciplity of infection (MOI) of
633 10 (PK15) or 5 (RK13). Titers represent mean values of three independent experiments
634 with standard deviation bars.

635 Figure 3

636 RT-qPCR expression kinetics of LLT during PrV infection *in vitro*. PK15 cells were infected
637 with pPrV-ΔmiRN (light gray) and pPrV-ΔgGG (dark gray) at a MOI of 10. Values are
638 provided as mean Ct values and are the average of three biological replicates (higher Ct
639 values mean decreased gene expression levels). The qPCRs were normalized to input
640 amount of total RNA.

641 Figure 4

642 Establishment of latency *in vivo*. Pigs were infected with either pPrV-ΔgGG (“WT” 54-58),
643 pPrV-ΔmiRN (“M” 49-53) or mock infected (“C” 43-48). A, B): DNAs from nasal swabs of
644 animals infected by WT PrV (A) or M PrV (B) were analyzed by RT-qPCR of the PRV gB
645 gene. C, D): The host antibody response was analyzed by ELISA using PrV gB as antigen.
646 The threshold value of the assay (0.7) is indicated as a red line.

647 Figure 5

648 Relative amounts of PrV genomes in latent trigeminal ganglia. A): The PrV genome copy
649 value per 100 ng of genomic DNA was quantified by qPCR using a GFP amplicon. B): PA-
650 GFP-coilin C2 plasmid DNA standard curve. The x-axis represents the input copies of

651 plasmid DNA and the y-axis the mean cycle of threshold (Ct mean).

652 Figure 6

653 RT-qPCR profiles of prv-miR-LLT1, prv-miR-LLT2 and prv-miR-LLT10 in (A) trigeminal
654 ganglia latent for the WT or M PrV and (B) in PK15 cells at 12h p.i. with the WT PrV.
655 Values are normalized against background and indicated as $2^{-\Delta Ct}$ (± standard deviation).

656 Figure 7

657 Pattern of transcription of three regions of LLT (exon 1, ex1/ex2 junction and exon 2) in
658 trigeminal ganglia latent for the WT or M PrV. RT-qPCR values were calibrated vs. the
659 relative amount of PrV genomes. Values are the $2^{-\Delta Ct}$ (± standard deviation) calculated
660 from three technical replicates.

661 Figure 8

662 Visualization of the distribution of RNAseq reads obtained by RNAseq profiling of
663 trigeminal ganglia latent for the mutant (M) or parental (WT) PrV on the PrV genome.

664 Figure 9

665 IL6, IFNG and TNF were identified by IPA as most significant upstream regulators (z
666 scores > 2) to explain the pattern of transcription of 20 DE genes, of which 15 belong to
667 the top IPA network “Cell-mediated Immune Response, Cellular Movement,
668 Hematological System Development and Function” (17 DE genes). Left: WT vs. C; right:
669 M vs. C. Numbers are the logFC values of each comparison.

670 Red: upregulated; green: downregulated; orange: leads to activation; blue: leads to
671 inhibition; yellow: finding inconsistent with state of downstream molecules; grey: effect not
672 predicted.

673

References

1. **Klupp BG, Hengartner CJ, Mettenleiter TC, Enquist LW.** 2004. Complete, annotated sequence of the pseudorabies virus genome. J Virol **78:**424-440.
2. **Szpara ML, Tafuri YR, Parsons L, Shamim SR, Verstrepen KJ, Legendre M, Enquist LW.** 2011. A wide extent of inter-strain diversity in virulent and vaccine strains of alphaherpesviruses. PLoS Pathog **7:**e1002282.
3. **Yu X, Zhou Z, Hu D, Zhang Q, Han T, Li X, Gu X, Yuan L, Zhang S, Wang B, Qu P, Liu J, Zhai X, Tian K.** 2014. Pathogenic pseudorabies virus, China, 2012. Emerg Infect Dis **20:**102-104.
4. **Enquist LW.** 1994. Infection of the mammalian nervous system by pseudorabies virus (PRV), p. 221 ' 231, vol. 5. Semin. Virol.
5. **Mettenleiter TC.** 2000. Aujeszky's disease (pseudorabies) virus: the virus and molecular pathogenesis--state of the art, June 1999. Vet Res **31:**99-115.
6. **Pomeranz LE, Reynolds AE, Hengartner CJ.** 2005. Molecular biology of pseudorabies virus: impact on neurovirology and veterinary medicine. Microbiol Mol Biol Rev **69:**462-500.
7. **Gutekunst DE, Pirtle EC, Miller LD, Stewart WC.** 1980. Isolation of pseudorabies virus from trigeminal ganglia of a latently infected sow. Am J Vet Res **41:**1315-1316.
8. **Cheung AK.** 1991. Cloning of the latency gene and the early protein 0 gene of pseudorabies virus. J Virol **65:**5260-5271.
9. **Priola SA, Gustafson DP, Wagner EK, Stevens JG.** 1990. A major portion of the latent pseudorabies virus genome is transcribed in trigeminal ganglia of pigs. J Virol **64:**4755-4760.
10. **Priola SA, Stevens JG.** 1991. The 5' and 3' limits of transcription in the pseudorabies virus latency associated transcription unit. Virology **182:**852-856.
11. **Cheung AK.** 1989. Detection of pseudorabies virus transcripts in trigeminal ganglia of latently infected swine. J Virol **63:**2908-2913.
12. **Jin L, Scherba G.** 1999. Expression of the pseudorabies virus latency-associated transcript gene during productive infection of cultured cells. J Virol **73:**9781-9788.
13. **Bartel DP.** 2004. MicroRNAs: genomics, biogenesis, mechanism, and function. Cell **116:**281-297.
14. **Yates LA, Norbury CJ, Gilbert RJ.** 2013. The long and short of microRNA. Cell **153:**516-519.

15. **Mendell JT, Olson EN.** 2012. MicroRNAs in stress signaling and human disease. Cell **148:**1172-1187.
16. **Skalsky RL, Cullen BR.** 2010. Viruses, microRNAs, and host interactions. Annu Rev Microbiol **64:**123-141.
17. **Cullen BR.** 2013. MicroRNAs as mediators of viral evasion of the immune system. Nat Immunol **14:**205-210.
18. **Jurak I, Griffiths A, Coen DM.** 2011. Mammalian alphaherpesvirus miRNAs. Biochim Biophys Acta **1809:**641-653.
19. **Pfeffer S, Zavolan M, Grässer FA, Chien M, Russo JJ, Ju J, John B, Enright AJ, Marks D, Sander C, Tuschl T.** 2004. Identification of virus-encoded microRNAs. Science **304:**734-736.
20. **Grundhoff A, Sullivan CS.** 2011. Virus-encoded microRNAs. Virology **411:**325-343.
21. **Tang Q, Wu YQ, Chen DS, Zhou Q, Chen HC, Liu ZF.** 2014. Bovine herpesvirus 5 encodes a unique pattern of microRNAs compared with bovine herpesvirus 1. J Gen Virol **95:**671-678.
22. **Anselmo A, Flori L, Jaffrezic F, Rutigliano T, Cecere M, Cortes-Perez N, Lefèvre F, Rogel-Gaillard C, Giuffra E.** 2011. Co-expression of host and viral microRNAs in porcine dendritic cells infected by the pseudorabies virus. PLoS One **6:**e17374.
23. **Wu YQ, Chen DJ, He HB, Chen DS, Chen LL, Chen HC, Liu ZF.** 2012. Pseudorabies virus infected porcine epithelial cell line generates a diverse set of host microRNAs and a special cluster of viral microRNAs. PLoS One **7:**e30988.
24. **Fuchs W, Backovic M, Klupp BG, Rey FA, Mettenleiter TC.** 2012. Structure-based mutational analysis of the highly conserved domain IV of glycoprotein H of pseudorabies virus. J Virol **86:**8002-8013.
25. **KAPLAN AS, VATTER AE.** 1959. A comparison of herpes simplex and pseudorabies viruses. Virology **7:**394-407.
26. **Grimm KS, Klupp BG, Granzow H, Müller FM, Fuchs W, Mettenleiter TC.** 2012. Analysis of viral and cellular factors influencing herpesvirus-induced nuclear envelope breakdown. J Virol **86:**6512-6521.
27. **Mettenleiter TC.** 1989. Glycoprotein gIII deletion mutants of pseudorabies virus are impaired in virus entry. Virology **171:**623-625.
28. **Wernike K, Beer M, Freuling CM, Klupp B, Mettenleiter TC, Müller T, Hoffmann B.** 2014. Molecular double-check strategy for the identification and characterization of Suid herpes virus 1. J Virol Methods.

29. **Schroeder A, Mueller O, Stocker S, Salowsky R, Leiber M, Gassmann M, Lightfoot S, Menzel W, Granzow M, Ragg T.** 2006. The RIN: an RNA integrity number for assigning integrity values to RNA measurements. BMC Mol Biol **7:**3.

30. **Thiery R, Pannetier C, Rziha HJ, Jestin A.** 1996. A fluorescence-based quantitative PCR method for investigation of pseudorabies virus latency. J Virol Methods **61:**79-87.

31. **Groenen MA, Archibald AL, Uenishi H, Tuggle CK, Takeuchi Y, Rothschild MF, Rogel-Gaillard C, Park C, Milan D, Megens HJ, Li S, Larkin DM, Kim H, Frantz LA, Caccamo M, Ahn H, Aken BL, Anselmo A, Anthon C, Auvil L, Badaoui B, Beattie CW, Bendixen C, Berman D, Blecha F, Blomberg J, Bolund L, Bosse M, Botti S, Bujie Z, Bystrom M, Capitanu B, Carvalho-Silva D, Chardon P, Chen C, Cheng R, Choi SH, Chow W, Clark RC, Clee C, Crooijmans RP, Dawson HD, Dehais P, De Sapio F, Dibbits B, Drou N, Du ZQ, Eversole K, Fadista J, Fairley S, Faraut T, Faulkner GJ, Fowler KE, Fredholm M, Fritz E, Gilbert JG, Giuffra E, Gorodkin J, Griffin DK, Harrow JL, Hayward A, Howe K, Hu ZL, Humphray SJ, Hunt T, Hornshøj H, Jeon JT, Jern P, Jones M, Jurka J, Kanamori H, Kapetanovic R, Kim J, Kim JH, Kim KW, Kim TH, Larson G, Lee K, Lee KT, Leggett R, Lewin HA, Li Y, Liu W, Loveland JE, Lu Y, Lunney JK, Ma J, Madsen O, Mann K, Matthews L, McLaren S, Morozumi T, Murtaugh MP, Narayan J, Nguyen DT, Ni P, Oh SJ, Onteru S, Panitz F, Park EW, Park HS, Pascal G, Paudel Y, Perez-Enciso M, Ramirez-Gonzalez R, Reecy JM, Rodriguez-Zas S, Rohrer GA, Rund L, Sang Y, Schachtschneider K, Schraiber JG, Schwartz J, Scobie L, Scott C, Searle S, Servin B, Southey BR, Sperber G, Stadler P, Sweedler JV, Tafer H, Thomsen B, Wali R, Wang J, White S, Xu X, Yerle M, Zhang G, Zhang J, Zhao S, Rogers J, Churcher C, Schook LB.** 2012. Analyses of pig genomes provide insight into porcine demography and evolution. Nature **491:**393-398.

32. **Anders S, Huber W.** 2010. Differential expression analysis for sequence count data. Genome Biol **11:**R106.

33. **Trapnell C, Roberts A, Goff L, Pertea G, Kim D, Kelley DR, Pimentel H, Salzberg SL, Rinn JL, Pachter L.** 2012. Differential gene and transcript expression analysis of RNA-seq experiments with TopHat and Cufflinks. Nat Protoc **7:**562-578.

34. **Robinson MD, McCarthy DJ, Smyth GK.** 2010. edgeR: a Bioconductor package for differential expression analysis of digital gene expression data. Bioinformatics **26:**139-140.

35. **Martin M.** 2011. Cutadapt removes adapter sequences from high-throughput sequencing reads., e47786 ed, vol. 7. EMBnet J.
36. **Friedländer MR, Mackowiak SD, Li N, Chen W, Rajewsky N.** 2012. miRDeep2 accurately identifies known and hundreds of novel microRNA genes in seven animal clades. Nucleic Acids Res **40:**37-52.
37. **Kozomara A, Griffiths-Jones S.** 2011. miRBase: integrating microRNA annotation and deep-sequencing data. Nucleic Acids Res **39:**D152-157.
38. **Tombácz D, Tóth JS, Petrovszki P, Boldogkoi Z.** 2009. Whole-genome analysis of pseudorabies virus gene expression by real-time quantitative RT-PCR assay. BMC Genomics **10:**491.
39. **Untergasser A, Nijveen H, Rao X, Bisseling T, Geurts R, Leunissen JA.** 2007. Primer3Plus, an enhanced web interface to Primer3. Nucleic Acids Res **35:**W71-74.
40. **Owczarzy R, You Y, Groth CL, Tataurov AV.** 2011. Stability and mismatch discrimination of locked nucleic acid-DNA duplexes. Biochemistry **50:**9352-9367.
41. **Chen C, Ridzon DA, Broomer AJ, Zhou Z, Lee DH, Nguyen JT, Barbisin M, Xu NL, Mahuvakar VR, Andersen MR, Lao KQ, Livak KJ, Guegler KJ.** 2005. Real-time quantification of microRNAs by stem-loop RT-PCR. Nucleic Acids Res **33:**e179.
42. **Lewis BP, Burge CB, Bartel DP.** 2005. Conserved seed pairing, often flanked by adenosines, indicates that thousands of human genes are microRNA targets. Cell **120:**15-20.
43. **Grimson A, Farh KK, Johnston WK, Garrett-Engele P, Lim LP, Bartel DP.** 2007. MicroRNA targeting specificity in mammals: determinants beyond seed pairing. Mol Cell **27:**91-105.
44. **Loveland JE, Gilbert JG, Griffiths E, Harrow JL.** 2012. Community gene annotation in practice. Database (Oxford) **2012:**bas009.
45. **Cohrs RJ, Randall J, Smith J, Gilden DH, Dabrowski C, van Der Keyl H, Tal-Singer R.** 2000. Analysis of individual human trigeminal ganglia for latent herpes simplex virus type 1 and varicella-zoster virus nucleic acids using real-time PCR. J Virol **74:**11464-11471.
46. **Keane TM, Goodstadt L, Danecek P, White MA, Wong K, Yalcin B, Heger A, Agam A, Slater G, Goodson M, Furlotte NA, Eskin E, Nellåker C, Whitley H, Cleak J, Janowitz D, Hernandez-Pliego P, Edwards A, Belgard TG, Oliver PL, McIntyre RE, Bhomra A, Nicod J, Gan X, Yuan W, van der Weyden L, Steward CA, Bala S, Stalker J, Mott R, Durbin R, Jackson IJ, Czechanski A, Guerra-Assunção JA,**

Donahue LR, Reinholdt LG, Payseur BA, Ponting CP, Birney E, Flint J, Adams DJ. 2011. Mouse genomic variation and its effect on phenotypes and gene regulation. Nature **477:**289-294.

47. **Fagerberg L, Hallström BM, Oksvold P, Kampf C, Djureinovic D, Odeberg J, Habuka M, Tahmasebpoor S, Danielsson A, Edlund K, Asplund A, Sjöstedt E, Lundberg E, Szigyarto CA, Skogs M, Takanen JO, Berling H, Tegel H, Mulder J, Nilsson P, Schwenk JM, Lindskog C, Danielsson F, Mardinoglu A, Sivertsson A, von Feilitzen K, Forsberg M, Zwahlen M, Olsson I, Navani S, Huss M, Nielsen J, Ponten F, Uhlén M.** 2014. Analysis of the human tissue-specific expression by genome-wide integration of transcriptomics and antibody-based proteomics. Mol Cell Proteomics **13:**397-406.

48. **Timoneda O, Núñez-Hernández F, Balcells I, Muñoz M, Castelló A, Vera G, Pérez LJ, Egea R, Mir G, Córdoba S, Rosell R, Segalés J, Tomàs A, Sánchez A, Núñez JI.** 2014. The role of viral and host microRNAs in the Aujeszky's disease virus during the infection process. PLoS One **9:**e86965.

49. **Cheung AK.** 1996. Latency characteristics of an EPO and LLT mutant of pseudorabies virus. J Vet Diagn Invest **8:**112-115.

50. **Cliffe AR, Garber DA, Knipe DM.** 2009. Transcription of the herpes simplex virus latency-associated transcript promotes the formation of facultative heterochromatin on lytic promoters. J Virol **83:**8182-8190.

51. **Wang QY, Zhou C, Johnson KE, Colgrove RC, Coen DM, Knipe DM.** 2005. Herpesviral latency-associated transcript gene promotes assembly of heterochromatin on viral lytic-gene promoters in latent infection. Proc Natl Acad Sci U S A **102:**16055-16059.

52. **Kramer MF, Jurak I, Pesola JM, Boissel S, Knipe DM, Coen DM.** 2011. Herpes simplex virus 1 microRNAs expressed abundantly during latent infection are not essential for latency in mouse trigeminal ganglia. Virology **417:**239-247.

53. **Roizman B, Whitley RJ.** 2013. An inquiry into the molecular basis of HSV latency and reactivation. Annu Rev Microbiol **67:**355-374.

54. **Bloom DC, Giordani NV, Kwiatkowski DL.** 2010. Epigenetic regulation of latent HSV-1 gene expression. Biochim Biophys Acta **1799:**246-256.

55. **Jurak I, Hackenberg M, Kim JY, Pesola JM, Everett RD, Preston CM, Wilson AC, Coen DM.** 2014. Expression of herpes simplex virus 1 microRNAs in cell culture models of quiescent and latent infection. J Virol **88:**2337-2339.

56. **Leib DA, Harrison TE, Laslo KM, Machalek MA, Moorman NJ, Virgin HW.** 1999. Interferons regulate the phenotype of wild-type and mutant herpes simplex viruses in vivo. J Exp Med **189:**663-672.

57. **Knickelbein JE, Khanna KM, Yee MB, Baty CJ, Kinchington PR, Hendricks RL.** 2008. Noncytotoxic lytic granule-mediated CD8+ T cell inhibition of HSV-1 reactivation from neuronal latency. Science **322:**268-271.

58. **Kristie TM, Vogel JL, Sears AE.** 1999. Nuclear localization of the C1 factor (host cell factor) in sensory neurons correlates with reactivation of herpes simplex virus from latency. Proc Natl Acad Sci U S A **96:**1229-1233.

59. **Chentoufi AA, Kritzer E, Tran MV, Dasgupta G, Lim CH, Yu DC, Afifi RE, Jiang X, Carpenter D, Osorio N, Hsiang C, Nesburn AB, Wechsler SL, BenMohamed L.** 2011. The herpes simplex virus 1 latency-associated transcript promotes functional exhaustion of virus-specific CD8+ T cells in latently infected trigeminal ganglia: a novel immune evasion mechanism. J Virol **85:**9127-9138.

60. **Chentoufi AA, Dervillez X, Dasgupta G, Nguyen C, Kabbara KW, Jiang X, Nesburn AB, Wechsler SL, Benmohamed L.** 2012. The herpes simplex virus type 1 latency-associated transcript inhibits phenotypic and functional maturation of dendritic cells. Viral Immunol **25:**204-215.

61. **Li JM, Southerland L, Hossain MS, Giver CR, Wang Y, Darlak K, Harris W, Waschek J, Waller EK.** 2011. Absence of vasoactive intestinal peptide expression in hematopoietic cells enhances Th1 polarization and antiviral immunity in mice. J Immunol **187:**1057-1065.

62. **Li JM, Darlak KA, Southerland L, Hossain MS, Jaye DL, Josephson CD, Rosenthal H, Waller EK.** 2013. VIPhyb, an antagonist of vasoactive intestinal peptide receptor, enhances cellular antiviral immunity in murine cytomegalovirus infected mice. PLoS One **8:**e63381.

63. **Renton KW, Nicholson TE.** 2000. Hepatic and central nervous system cytochrome P450 are down-regulated during lipopolysaccharide-evoked localized inflammation in brain. J Pharmacol Exp Ther **294:**524-530.

64. **Henry J, Miller MM, Pontarotti P.** 1999. Structure and evolution of the extended B7 family. Immunol Today **20:**285-288.

65. **Afrache H, Gouret P, Ainouche S, Pontarotti P, Olive D.** 2012. The butyrophilin (BTN) gene family: from milk fat to the regulation of the immune response. Immunogenetics **64:**781-794.

66. **Abeler-Dörner L, Swamy M, Williams G, Hayday AC, Bas A.** 2012. Butyrophilins: an emerging family of immune regulators. Trends Immunol **33:**34-41.
67. **Cliffe AR, Coen DM, Knipe DM.** 2013. Kinetics of facultative heterochromatin and polycomb group protein association with the herpes simplex viral genome during establishment of latent infection. MBio **4**.

Table 1. Descriptive statistics of Small RNA profiling of porcine trigeminal ganglia latent for either the WT (parental) or M (mutant) PrV. Thirteen individual small RNAseq libraries were constructed from five WT-infected animals (54 WT, 55 WT, 56 WT, 57 WT, 58 WT), five M-infected animals (49M, 50 M, 51 M, 52 M, 53 M) and three mock-infected animals (22 C, 23 C, 25C). Values are indicated as millions of normalized reads. The average counts are provided at the bottom of each column.

Samples	Reads mapping on miRNAs	Reads <16nt and >29nt	Total reads
22 C	7.8	16.9	42.9
23 C	5.8	8.7	46.8
25 C	7.2	12.9	27.3
49 M	6.9	14.8	55.3
50 M	20.7	34.7	47.9
51 M	11.3	17.7	43.8
52 M	16	15.9	46.1
53 M	16.3	19.8	39.2
54 WT	10	8	20.7
55 WT	5.7	16.5	27.4
56 WT	25.6	32.8	46.5
57 WT	15	19	20.7
58 WT	13.5	15.9	28.4
	12.4 ± 6.1	**18.0 ± 7.8**	**37.9 ± 11.5**

Table 2. Expression levels of PrV miRNAs in trigeminal ganglia latent for the WT or M PrV. In bold the miRNAs deleted in the M genome. Both prv-mir-LLT10 and prv-mir-LLT11 are duplicated in PrV genome as identical genes (prv-mir-LLT10a and prv-mir-LLT10b; prv-mir-LLT11a and prv-mir-LLT11b). Values are provided as counts per million of reads (cpm).

microRNA name	miRBase ID	miRBase Accession number	mature miRNA sequence (5'-3')	54 WT	55 WT	56 WT	57 WT	58 WT	49 M	50 M	51 M	52 M	53 M
prv-mir-LLT1-5p			GACGGCTCCTGGGGCTGAAAGC	0.18	0.60	1.84	0.27	0.15	-	-	-	-	-
prv-mir-LLT1-3p	**prv-miR-LLT1**	**MIMAT0025304**	UCUCACCCCUGGGUCCGUCGC	25.11	43.27	76.90	5.54	17.18	-	-	-	-	-
prv-mir-LLT2-5p	**prv-miR-LLT2**	**MIMAT0025305**	CUCAUCCCGUCAGACCUGCG	55.17	344.02	153.63	14.34	35.02	-	-	-	-	-
prv-mir-LLT2-3p			CGCGGGGCAACGGTGGTGAG	0.35	-	0.31	0.13	0.07	-	-	-	-	-
prv-mir-LLT3-5p			GAGCCGGGGGGGTCGAGTG	-	-	-	-	-	-	-	-	-	-
prv-mir-LLT3-3p	**prv-miR-LLT3**	**MIMAT0025306**	CGCACACGCCCCUCUCGCGCAC	0.18	0.70	1.80	-	0.37	-	-	-	-	-
prv-mir-LLT4-5p	**prv-miR-LLT4**	**MIMAT0025307**	AGAGUAUCAGCGUGGCUUUUUU	4.42	4.59	23.07	1.40	2.59	-	-	-	-	-
prv-mir-LLT4-3p			AAAAGGCACGCTGATGCGTCC	-	-	0.12	-	-	-	-	-	-	-
prv-mir-LLT5-5p				-	-	-	-	-	-	-	-	-	-
prv-mir-LLT5-3p	**prv-miR-LLT5**	**MIMAT0025308**	UGAGUGGAUGGAUGGAGGCGAG	-	0.50	1.21	0.20	-	-	-	-	-	-
prv-mir-LLT6-5p	**prv-miR-LLT6**	**MIMAT0025309**	CGUACCGACCCGCCUACCAGG	-	3.39	1.02	-	-	-	-	-	-	-
prv-mir-LLT6-3p			CTTGGCAGCGGGTGGGTACC	-	0.80	0.70	0.07	0.22	-	-	-	-	-
prv-mir-LLT7-5p	**prv-miR-LLT7**	**MIMAT0025310**	CCGGGGGGUUGAUGGGGAU	-	-	-	-	-	-	-	-	-	-
prv-mir-LLT7-3p			ACCACCGTCCCCCTGTCCCT	1.42	4.29	5.70	2.27	2.00	-	-	-	-	-
prv-mir-LLT8-5p	**prv-miR-LLT8**	**MIMAT0025311**	GUGGGGGCGAAGAUUGGGUU	-	-	1.84	0.07	-	-	-	-	-	-
prv-mir-LLT8-3p			CAACCCTTCTGGAGCCCTACC	10.79	8.57	30.25	2.27	5.48	-	-	-	-	-
prv-mir-LLT9-5p	**prv-miR-LLT9**	**MIMAT0025312**	AUCGAGGAGAUGUGGAGGGG	-	0.20	0.59	-	0.07	-	-	-	-	-
prv-mir-LLT9-3p			CCCTCCCCCGCATCTCTTCTC	-	-	0.43	0.13	-	-	-	-	-	-
prv-mir-LLT10b-5p				-	-	-	-	-	0.15	-	-	-	-
prv-mir-LLT10b-3p	prv-miR-LLT10a prv-miR-LLT10b	MIMAT0025313 MIMAT0025314	CCGAGCCUGCCCCUUCCGUCGCA	24.05	51.74	74.05	4.47	10.51	18.93	4.68	11.13	17.36	75.16
prv-mir-LLT11b-5p	prv-miR-LLT11a prv-miR-LLT11b	MIMAT0025315 MIMAT0025316	AGGCUGGGAGUGGGGACGGAAGA	0.18	-	1.02	0.13	-	-	-	-	0.08	0.37
prv-mir-LLT11b-3p				-	0.80	1.17	0.07	0.07	-	0.05	-	-	0.25

Table 3. Comparison of RNAseq and RT-qPCR data of 16 genes differentially expressed in trigeminal ganglia latent for the WT or M PrV. Values are reported as fold change (logFC) for each of the three pairwise comparisons (WT vs. C, M vs. C, and M vs. WT). VIP was only detected in three M-ganglia samples.

			WT vs. C		M vs. C		M vs. WT	
Accession number	**Gene symbol**	**Gene name**	**RNAseq**	**RT-qPCR**	**RNAseq**	**RT-qPCR**	**RNAseq**	**RT-qPCR**
ENSSSCG00000028488	LTC4S	Leukotriene (LT) C(4) synthase	-1.38 *	-0.23	-0.72	-0.76	0.66	0.52
ENSSSCG00000013022	PYGM	Phosphorylase	-1.46 *	-0.88	-0.33	0.32	1.13	1.20 **
ENSSSCG00000010506	Opalin	Opalin (specifically expressed in brain)	-3.11 *	-3.06	-0.67	-0.40	2.44	2.66 *
ENSSSCG00000025434	CGA	Glycoprotein hormones alpha chain	-3.13 *	-2.27 *	-0.38	-0.72	2.75	1.55 *
ENSSSCG00000016664	NPSR1	Member of G-protein coupled receptor 1 family	-2.66 *	-0.27	-2.26	0.58	0.40	0.85
ENSSSCG00000003345	TMEM88B	Transmembrane protein 88B	-1.98 *	-1.29 *	-0.84	0.01	1.14	1.31 **
ENSSSCG00000000133	TST	Sulfurtransferase	-0.88 *	-0.74	-0.16	-0.02	0.73	0.72 *
ENSSSCG00000008648	RSAD2	Viperin antiviral protein	1.36 **	1.29	0.62	1.09	-0.73	-0.20
ENSSSCG00000003497	PLA2G2D	Phospholipase A2. group IID	1.30	0.70 *	2.25 **	1.31 *	0.95	0.61
ENSSSCG00000008217	CD8A	T-cell surface glycoprotein CD8 alpha chain	0.50	-0.31	1.37 *	1.10 *	0.87	1.41 **
ENSSSCG00000023489	CXCL9	Chemokine (C-X-C motif) ligand 9	0.81	1.02	1.92 ***	2.28 *	1.12	1.26 *
ENSSSCG00000010780	CYP2E1	Cytochrome P450 2E1	-2.28	-1.41	0.78	0.81	3.06 *	2.23 **
ENSSSCG00000025614	PRICKLE4	LIM protein famly member	-1.14	-0.15	1.56	0.56 *	2.71 *	0.71 *
ENSSSCG00000004492	SLC14A1	Membrane transporter of urea in erythrocytes	-1.96 ***	-1.32 *	-0.33	0.34	1.63 **	1.66 **
ENSSSCG00000009672	SCARA5	A ferritin receptor mediating non-transferrin iron delivery	-0.77 *	-0.73	0.27	0.16	1.05 ***	0.89 *
ENSSSCG00000004078	VIP	Vasointestinal neuropeptide	-	-	-	-	5.85 **	6.66 *

*: p≤0.05; **: p ≤0.01; ***: p ≤ 0.001.

Table 4. Diseases and biofunctions in trigeminal ganglia latent for M or WT PrV. The “M vs. C” and “WT vs. C” columns report the IPA z-scores of activation (positive values) or inhibition (negative values) in the two comparisons. The most different ones (in italic) are reported in bold on top (more inhibited/less activated in M) and bottom (more activated/less inhibited in M). The most significant p-values of each biofunction are in bold.

Diseases and Bio Functions	M vs C	WT vs C	p-Value	Genes
inflammation of organ	-1.17	1.05	1.38E-03	AGT,CD8A,CXCL9,CXCL13,CYP2E1,GPD1,ICOS,SCARA5,TNFRSF10B,VIP
inflammatory response	0.26	1.61	3.15E-03	AGT,CXCL13,CXCL9,ITGA2,PLA2G2D,SCARA5,VIP
cell death of T lymphocytes	-0.42	0.91	9.16E-03	GZMA,ICOS,LAG3,VIP
migration of dendritic cells	-0.69	0.44	**6.77E-06**	AGT,CXCL13,CXCL9,ICOS,VIP
recruitment of cells	-0.10	0.93	1.79E-03	AGT,CD8A,CXCL9,CXCL13,VIP
activation of T lymphocytes	0.52	1.56	2.45E-03	CD8A,GZMA,ICOS,LAG3,VIP
recruitment of lymphocytes	0.25	1.10	**4.88E-05**	AGT, CD8A, CXCL9, VIP
recruitment of granulocytes	-1.10	-0.25	1.57E-03	AGT, CD8A, CXCL9, VIP
cell movement of leukocytes	-0.46	0.29	1.07E-03	AGT,CD8A,CXCL9,CXCL13,ICOS,LAG3,LTC4S,VIP
survival of organism	-2.06	-1.34	**5.00E-04**	AGT, CD8A, CXCL9, GZMA, LAG3, RSAD2, SLC14A1, VIP
infiltration by mononuclear leukocytes	-0.62	0.06	**6.45E-05**	AGT,CXCL9,ICOS,LAG3,VIP
leukocyte migration	0.17	0.80	**6.04E-04**	AGT,CD8A,CXCL9,CXCL13,ICOS,ITGA2,LAG3,LTC4S,VIP
infiltration of leukocytes	-0.94	-0.32	**4.68E-04**	AGT,CXCL9,ICOS,LAG3,LTC4S,VIP
cell movement of T lymphocytes	-0.54	0.05	**1.43E-05**	AGT,CXCL9,CXCL13,ICOS,LAG3,VIP
Lymphocyte migration	0.25	0.77	**2.06E-05**	AGT,CD8A,CXCL9,CXCL13,ICOS,LAG3,VIP
activation of cells	0.65	1.15	**3.02E-04**	AGT,CD8A,CXCL9,GABRA1,GZMA,ICOS,LAG3,PLA2G2D,TNFRSF10B,VIP
activation of leukocytes	0.42	0.91	**6.25E-05**	AGT,CD8A,CXCL9,GZMA,ICOS,LAG3,PLA2G2D,TNFRSF10B,VIP
quantity of IgG	2.19	2.19	4.04E-03	CXCL9, ICOS, IGJ, IGLL1/IGLL5, RSAD2
binding of blood cells	1.87	1.87	2.44E-03	CXCL9, CXCL13, ICOS, ITGA2
binding of cells	1.60	1.60	**2.87E-04**	AGT,CXCL9,CXCL13,ICOS,ITGA2,SCARA5,VIP
differentiation of blood cells	0.42	0.42	4.51E-03	AGT,CD8A,ICOS,IGLL1/IGLL5,RSAD2,TNFRSF10B,VIP
accumulation of leukocytes	-0.46	-0.46	**4.47E-04**	AGT,CXCL9,ICOS,ITGA2,LTC4S
quantity of helper T lymphocytes	-0.57	-0.57	1.35E-03	CD8A, ICOS, LAG3, PLA2G2D
activation of phagocytes	-0.69	-0.69	8.01E-03	AGT,GZMA,PLA2G2D,TNFRSF10B
quantity of antigen presenting cells	-1.07	-1.07	4.34E-03	AGT,CXCL13,LTC4S,PLA2G2D
transport of molecule	-1.22	-1.39	2.94E-03	AGT,CD8A,CGA,CYP2E1,EPHX1,GABRA1,ICOS,MX2,RSAD2,SLC14A1,VIP
secretion of molecule	-1.22	-1.41	**4.84E-04**	AGT,CD8A,CGA,CYP2E1,ICOS,RSAD2,VIP
flux of Ca2+	0.91	0.54	**6.80E-04**	AGT,CD8A,CXCL13,ICOS,VIP
cellular homeostasis	-0.29	-0.66	**4.68E-06**	AGT,CD8A,CXCL13,CYP2E1,GABRA1,GZMA,ICOS,LAG3,MTNR1B,PYGM,RSAD2,SCARA5,SLC14A1,TNFRSF10B,VIP
production of reactive oxygen species	-0.09	-0.60	2.35E-03	AGT,CXCL9,CYP2E1,GZMA,VIP
ion homeostasis of cells	0.25	-0.25	**9.97E-06**	AGT,CD8A,CXCL13,GABRA1,ICOS,PYGM,SCARA5,SLC14A1,VIP
quantity of cells	0.42	-0.18	**7.95E-04**	AGT,CD8A,CGA,CXCL13,GABRA1,ICOS,IGJ,IGLL1/IGLL5,LAG3,LTC4S,PLA2G2D,SLC14A1,VIP
quantity of blood cells	0.78	0.14	**1.32E-04**	AGT,CD8A,CXCL13,ICOS,IGJ,IGLL1/IGLL5,LAG3,LTC4S,PLA2G2D,SLC14A1,VIP
mobilization of Ca2+	0.18	-0.46	**2.74E-04**	AGT,CD8A,CXCL9,CXCL13,NPSR1,VIP
quantity of leukocytes	0.58	-0.07	**2.09E-04**	AGT,CD8A,CXCL13,ICOS,IGJ,IGLL1/IGLL5,LAG3,LTC4S,PLA2G2D,VIP
quantity of lymphocytes	0.98	0.26	**1.31E-04**	AGT,CD8A,CXCL13,ICOS,IGJ,IGLL1/IGLL5,LAG3,PLA2G2D,VIP
quantity of T lymphocytes	0.02	-0.85	3.46E-03	AGT,CD8A,ICOS,LAG3,PLA2G2D,VIP
proliferation of lymphocytes	1.97	1.03	3.33E-03	BTNL9,CD8A,ICOS,IGLL1/IGLL5,LAG3,TNFRSF10B,VIP
quantity of Ca2+	0.99	0.01	4.55E-03	AGT,CD8A,CXCL9,CXCL13,VIP
synthesis of fatty acid	-0.14	-1.14	7.55E-03	AGT,CYP2E1,LTC4S,PLA2G2D
stimulation of cells	0.88	-0.13	**8.85E-04**	AGT,BTNL9,CD8A,ICOS,VIP
expansion of T lymphocytes	1.70	0.27	**3.88E-04**	BTNL9,ICOS,LAG3,VIP
concentration of fatty acid	-0.28	-1.94	5.64E-03	AGT,CYP2E1,LTC4S,VIP

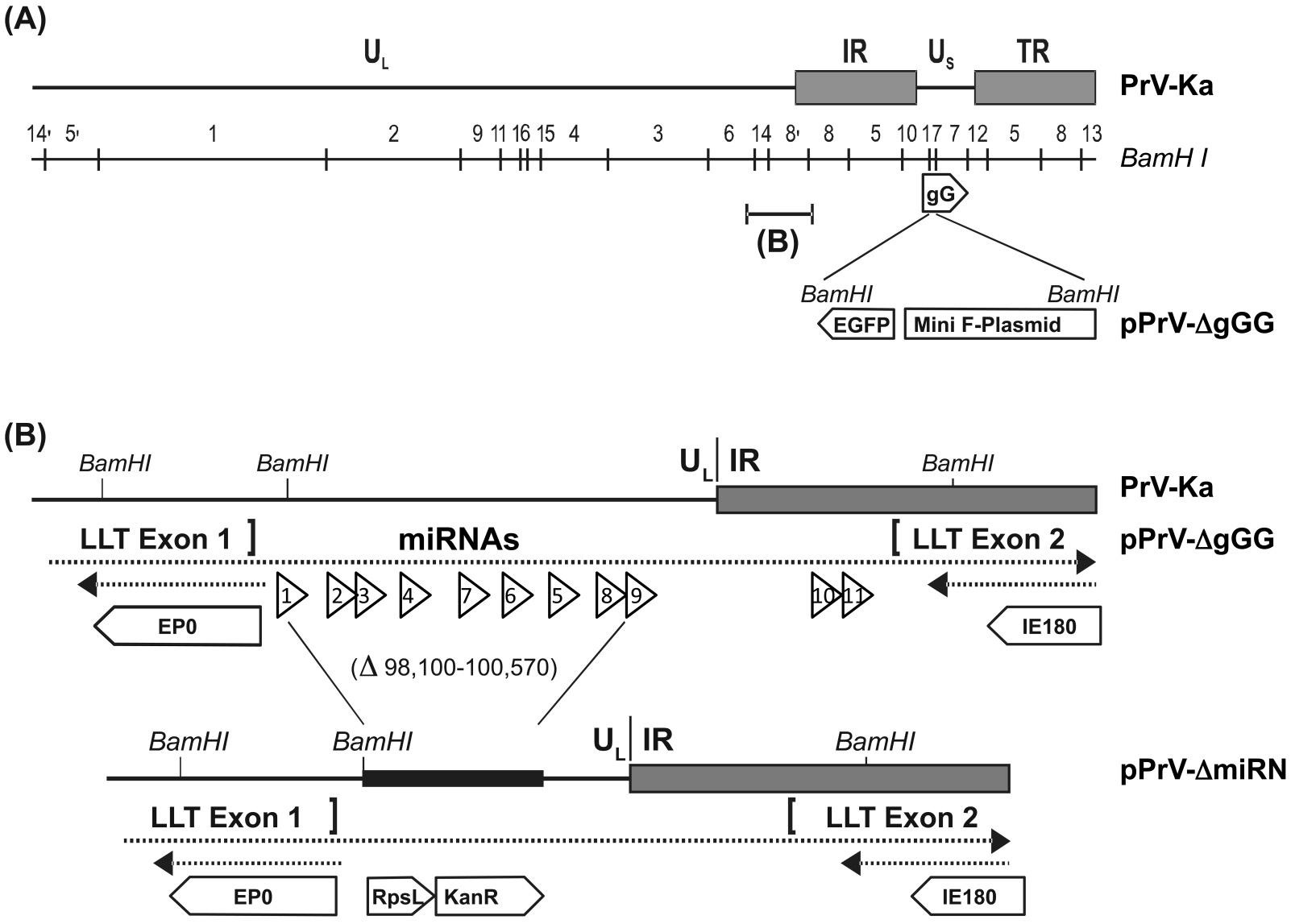
(A)
U_L
IR
U_S
TR
PrV-Ka
14' 5' 1 2 9 11 16 15 4 3 6 14 8' 8 5 10 17 7 12 5 8 13
BamH I
gG
(B)
BamHI
BamHI
EGFP
Mini F-Plasmid
pPrV-ΔgGG
(B)
BamHI
BamHI
U_L
IR
BamHI
PrV-Ka
LLT Exon 1
miRNAs
LLT Exon 2
pPrV-ΔgGG
1 2 3 4 7 6 5 8 9 10 11
EP0
IE180
(Δ 98,100-100,570)
BamHI
BamHI
U_L
IR
BamHI
pPrV-ΔmiRN
LLT Exon 1
LLT Exon 2
EP0
RpsL
KanR
IE180

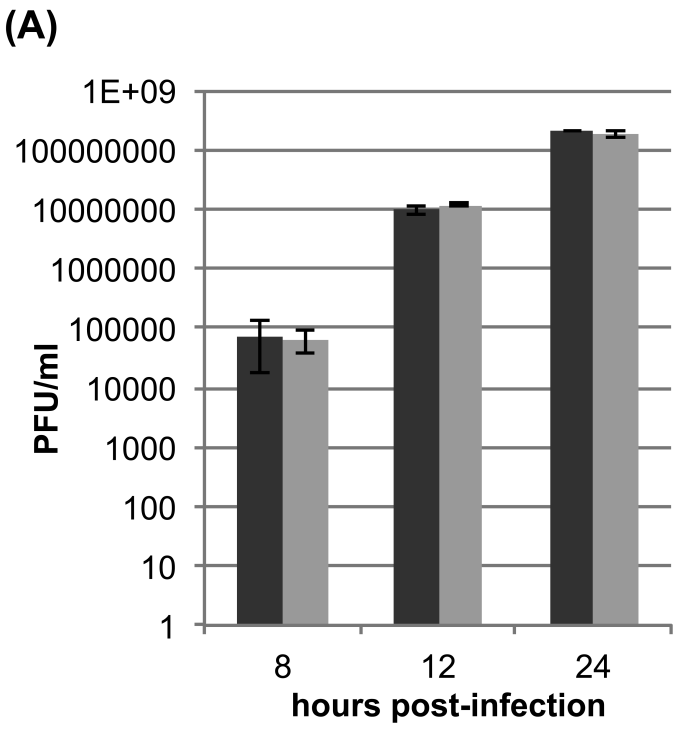
(A)
1E+09
100000000
10000000
1000000
100000
10000
1000
100
10
1
PFU/ml
8
12
24
hours post-infection

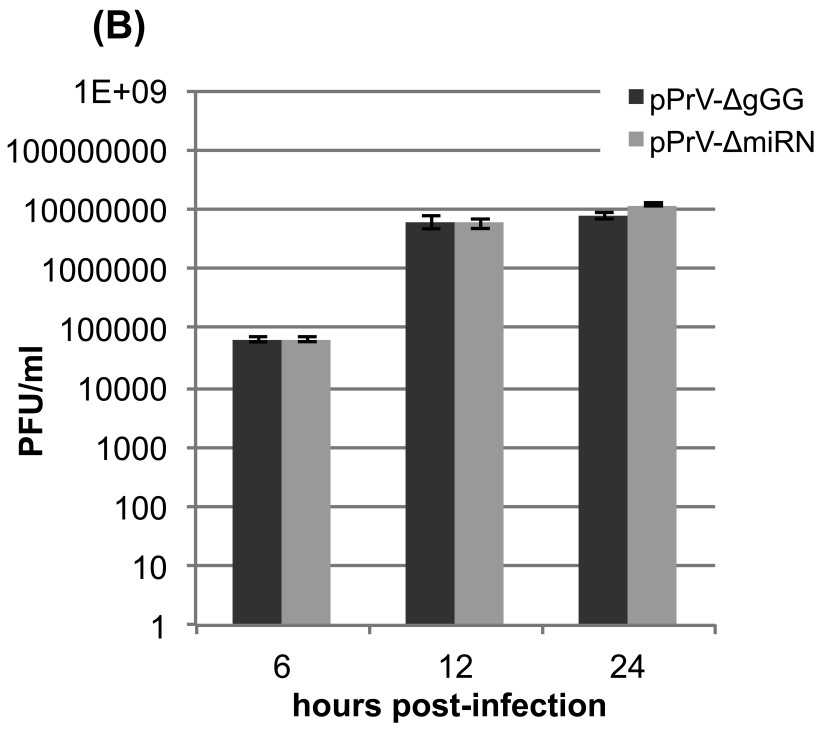
(B)
pPrV-ΔgGG
pPrV-ΔmiRN
1E+09
100000000
10000000
1000000
100000
10000
1000
100
10
1
PFU/ml
6
12
24
hours post-infection

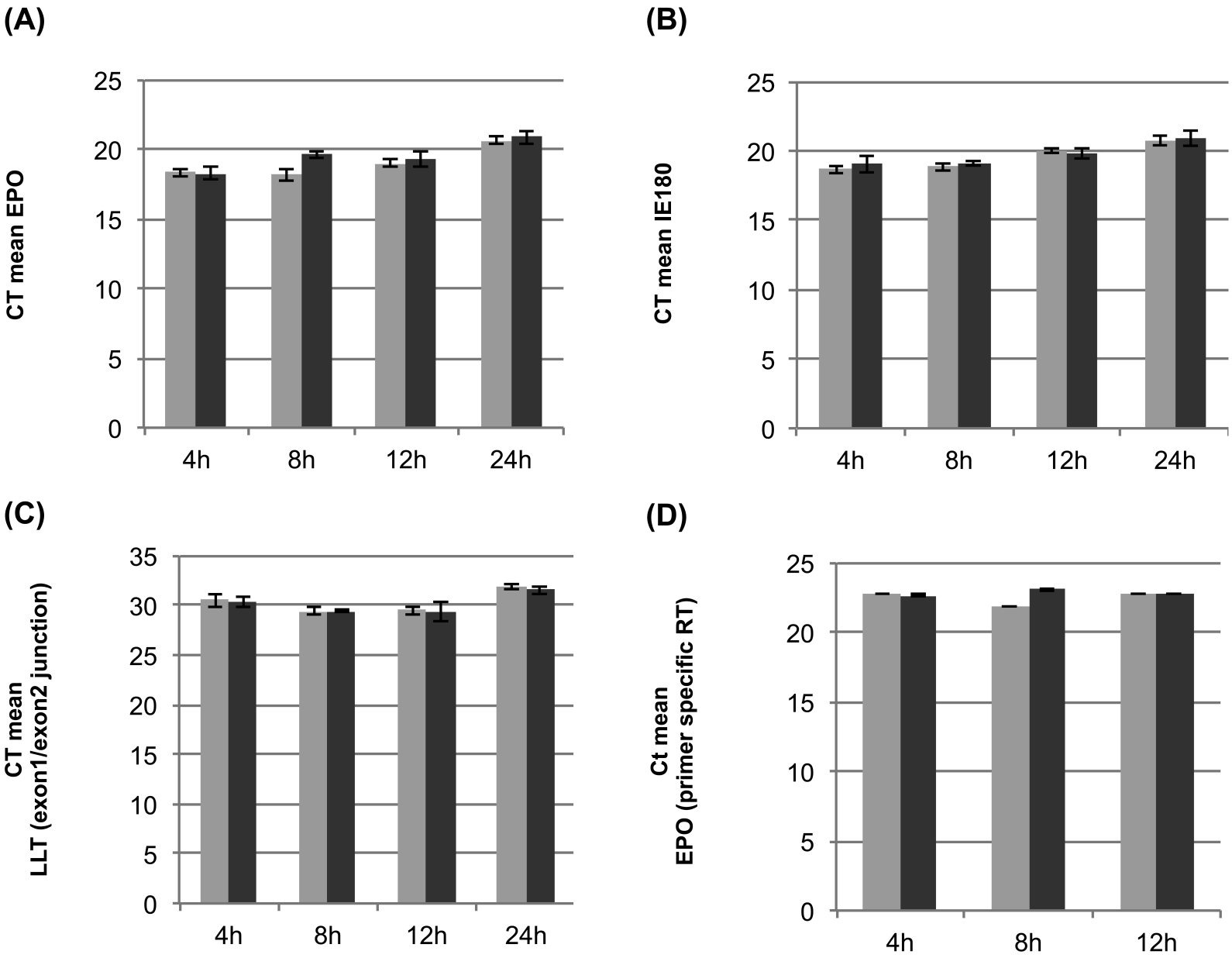
(A)
CT mean EPO
25
20
15
10
5
0
4h
8h
12h
24h
(B)
CT mean IE180
25
20
15
10
5
0
4h
8h
12h
24h
(C)
CT mean
LLT (exon1/exon2 junction)
35
30
25
20
15
10
5
0
4h
8h
12h
24h
(D)
Ct mean
EPO (primer specific RT)
25
20
15
10
5
0
4h
8h
12h

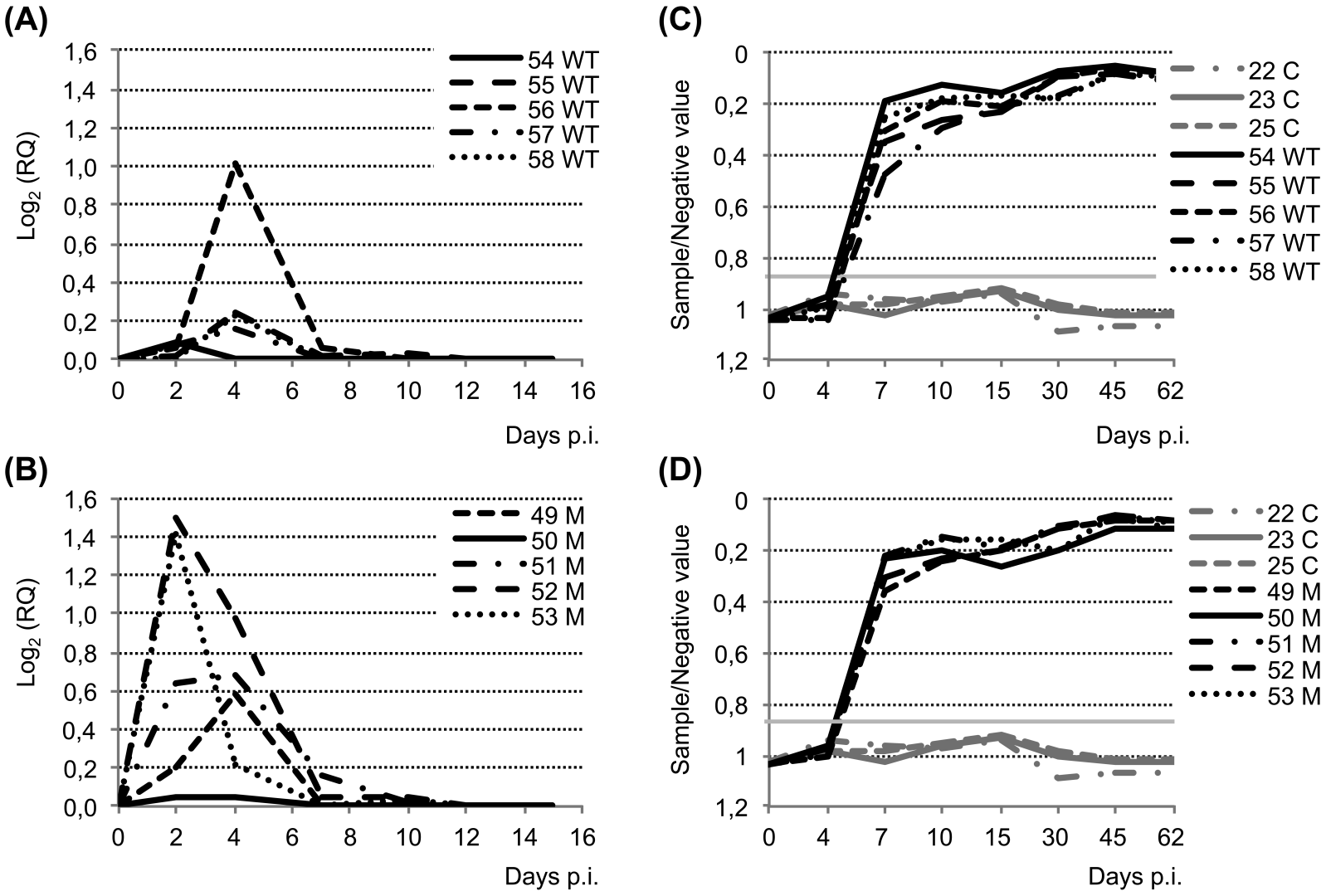
(A)
Log2 (RQ)
1,6
1,4
1,2
1,0
0,8
0,6
0,4
0,2
0,0
0 2 4 6 8 10 12 14 16
Days p.i.
54 WT
55 WT
56 WT
57 WT
58 WT
(B)
Log2 (RQ)
1,6
1,4
1,2
1,0
0,8
0,6
0,4
0,2
0,0
0 2 4 6 8 10 12 14 16
Days p.i.
49 M
50 M
51 M
52 M
53 M
(C)
Sample/Negative value
0
0,2
0,4
0,6
0,8
1
1,2
0 4 7 10 15 30 45 62
Days p.i.
22 C
23 C
25 C
54 WT
55 WT
56 WT
57 WT
58 WT
(D)
Sample/Negative value
0
0,2
0,4
0,6
0,8
1
1,2
0 4 7 10 15 30 45 62
Days p.i.
22 C
23 C
25 C
49 M
50 M
51 M
52 M
53 M

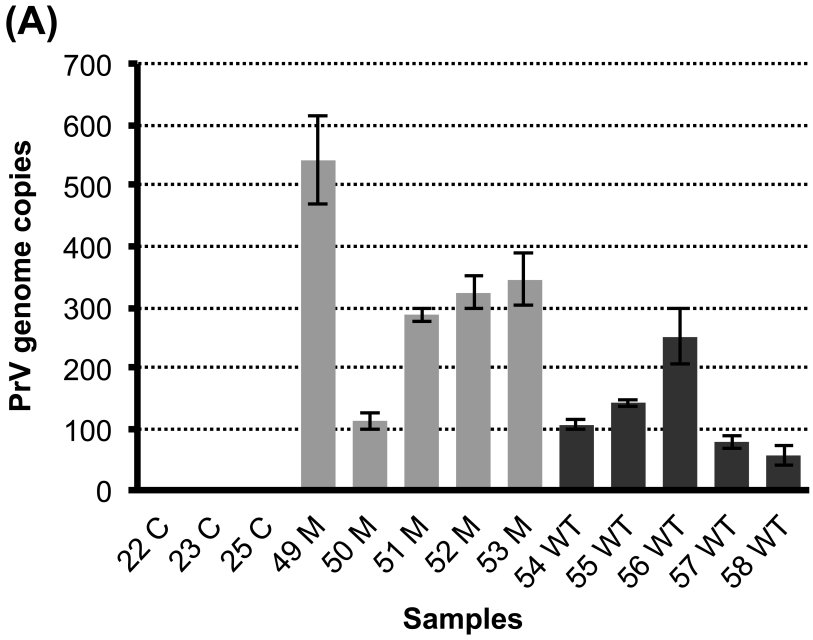
(A)
PrV genome copies
700
600
500
400
300
200
100
0
22 C
23 C
25 C
49 M
50 M
51 M
52 M
53 M
54 WT
55 WT
56 WT
57 WT
58 WT
Samples

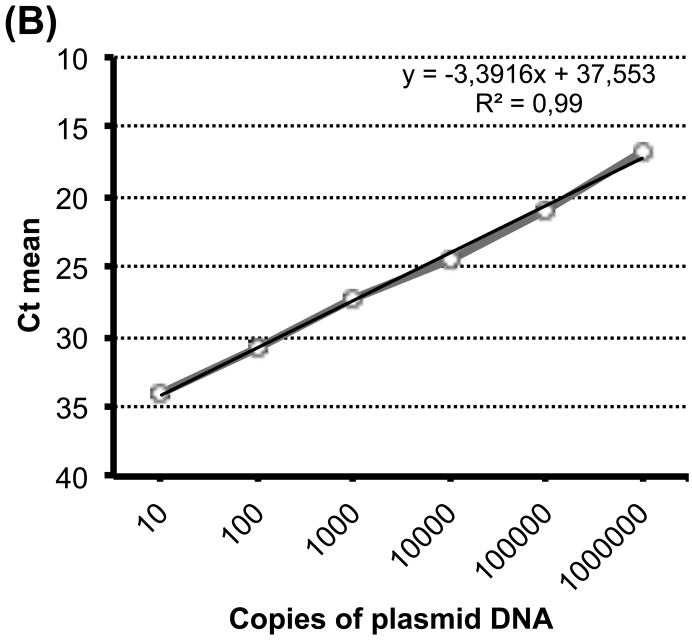
(B)
y = -3,3916x + 37,553
R² = 0,99
Ct mean
10
15
20
25
30
35
40
10
100
1000
10000
100000
1000000
Copies of plasmid DNA

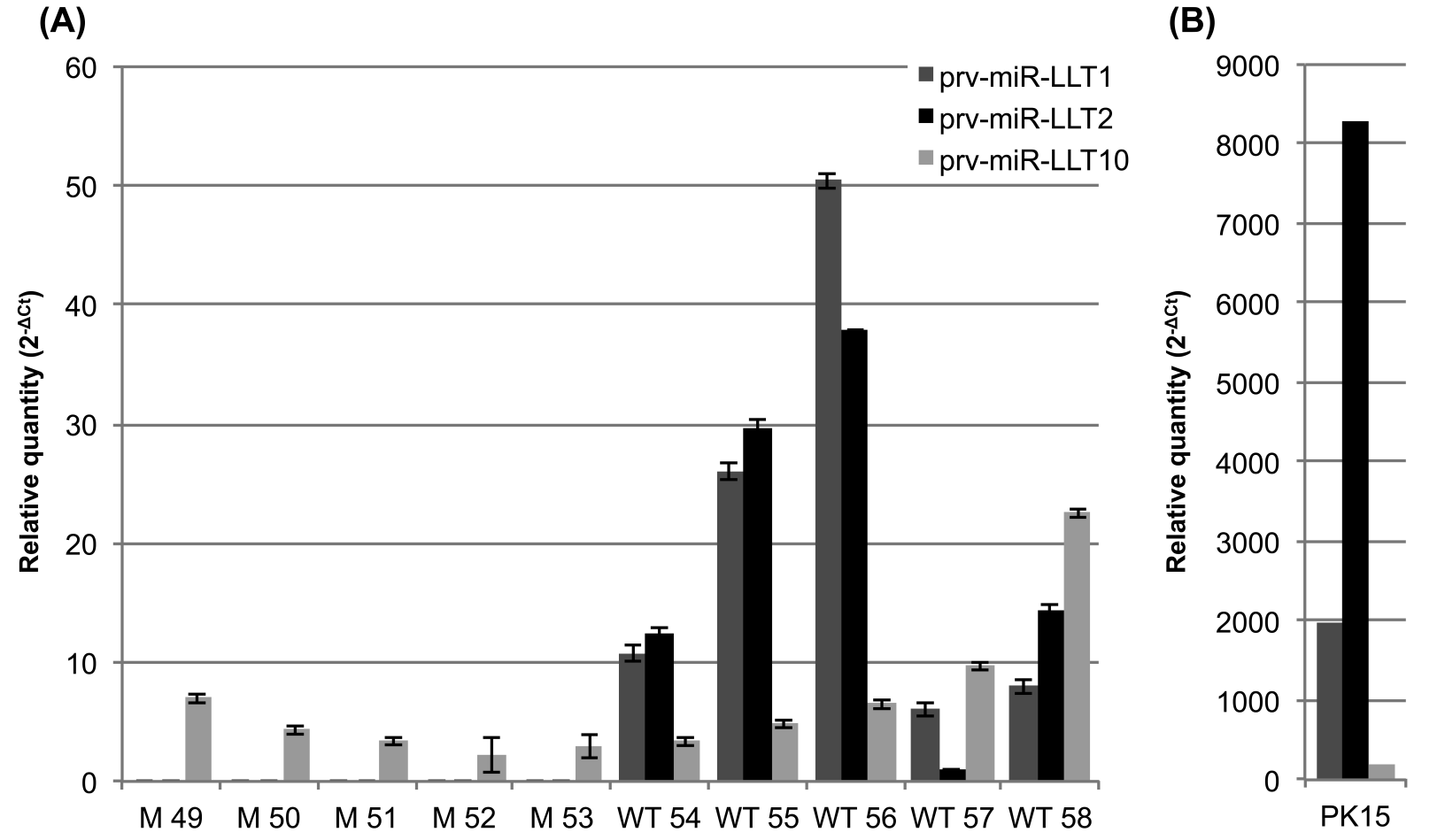
(A)
(B)
prv-miR-LLT1
prv-miR-LLT2
prv-miR-LLT10
Relative quantity (2-ΔCt)
60
50
40
30
20
10
0
M 49
M 50
M 51
M 52
M 53
WT 54
WT 55
WT 56
WT 57
WT 58
9000
8000
7000
6000
5000
4000
3000
2000
1000
0
PK15

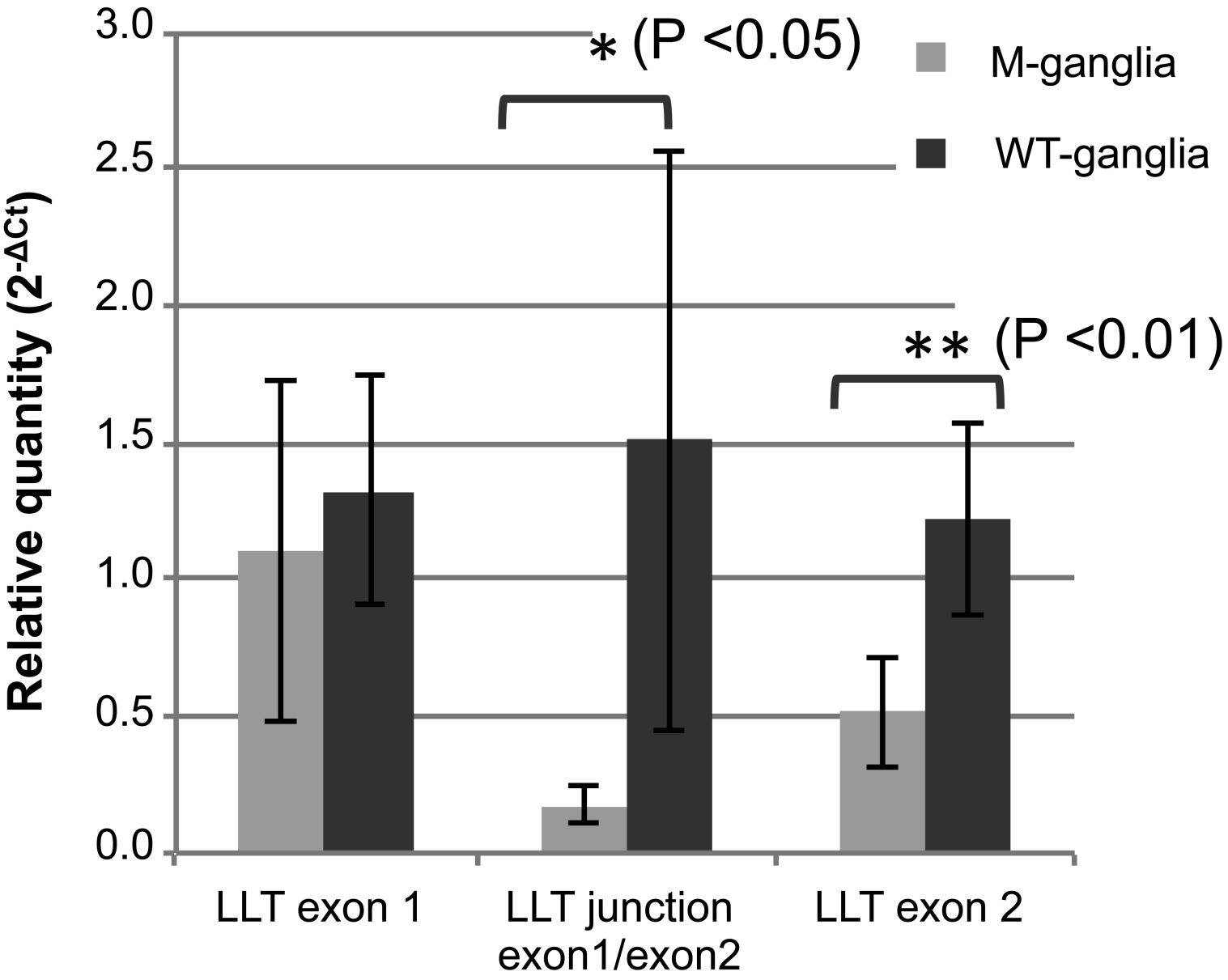
3.0
2.5
2.0
1.5
1.0
0.5
0.0
Relative quantity (2-ΔCt)
* (P <0.05)
** (P <0.01)
M-ganglia
WT-ganglia
LLT exon 1
LLT junction exon1/exon2
LLT exon 2

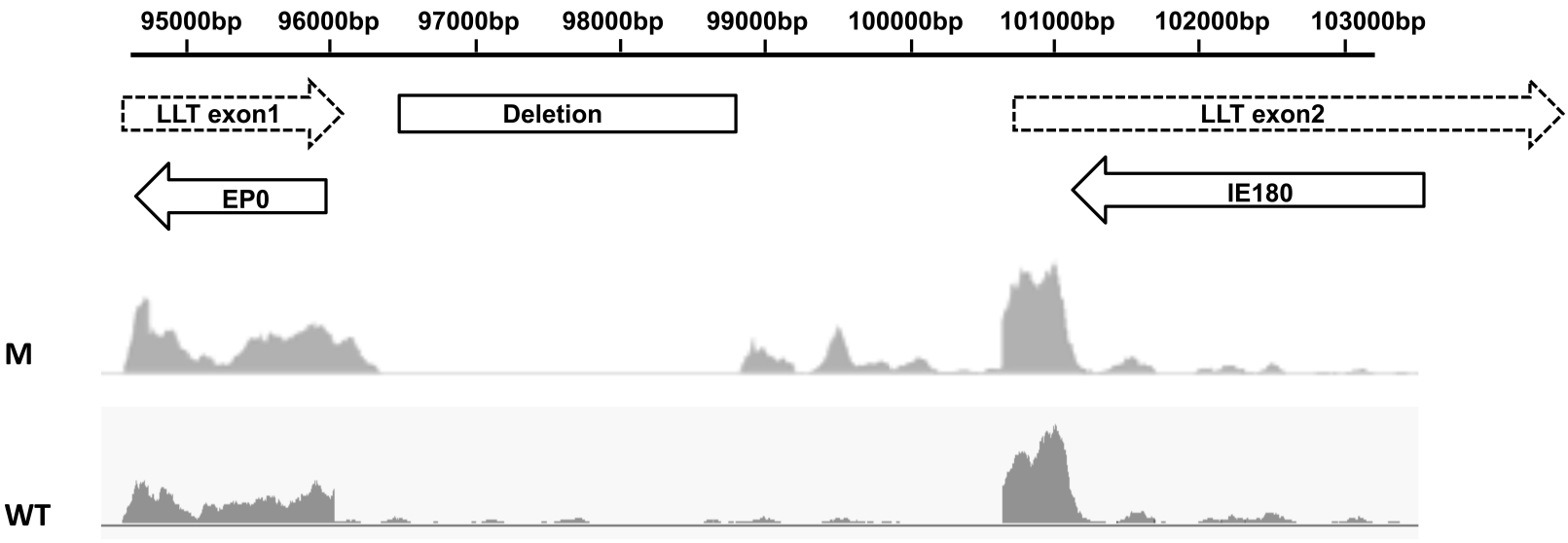
95000bp
96000bp
97000bp
98000bp
99000bp
100000bp
101000bp
102000bp
103000bp
LLT exon1
Deletion
LLT exon2
EP0
IE180
M
WT

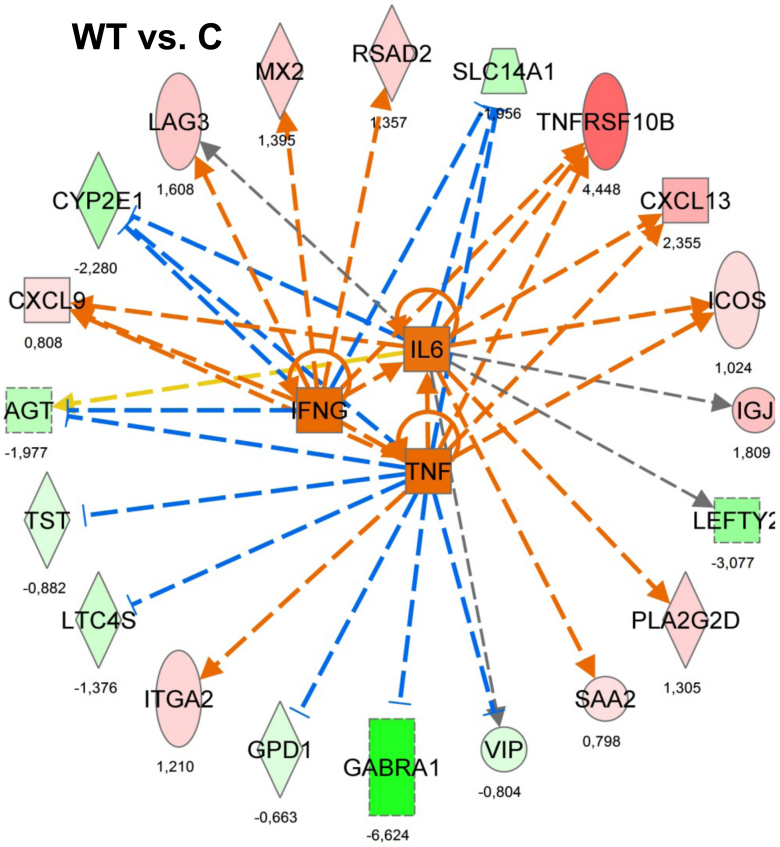
WT vs. C
MX2
1,395
RSAD2
1,357
SLC14A1
1,956
LAG3
1,608
TNFRSF10B
4,448
CYP2E1
-2,280
CXCL13
2,355
CXCL9
0,808
ICOS
1,024
IL6
IFNG
AGT
-1,977
IGJ
1,809
TNF
TST
-0,882
LEFTY2
-3,077
LTC4S
-1,376
PLA2G2D
1,305
ITGA2
1,210
SAA2
0,798
GPD1
-0,663
GABRA1
-6,624
VIP
-0,804

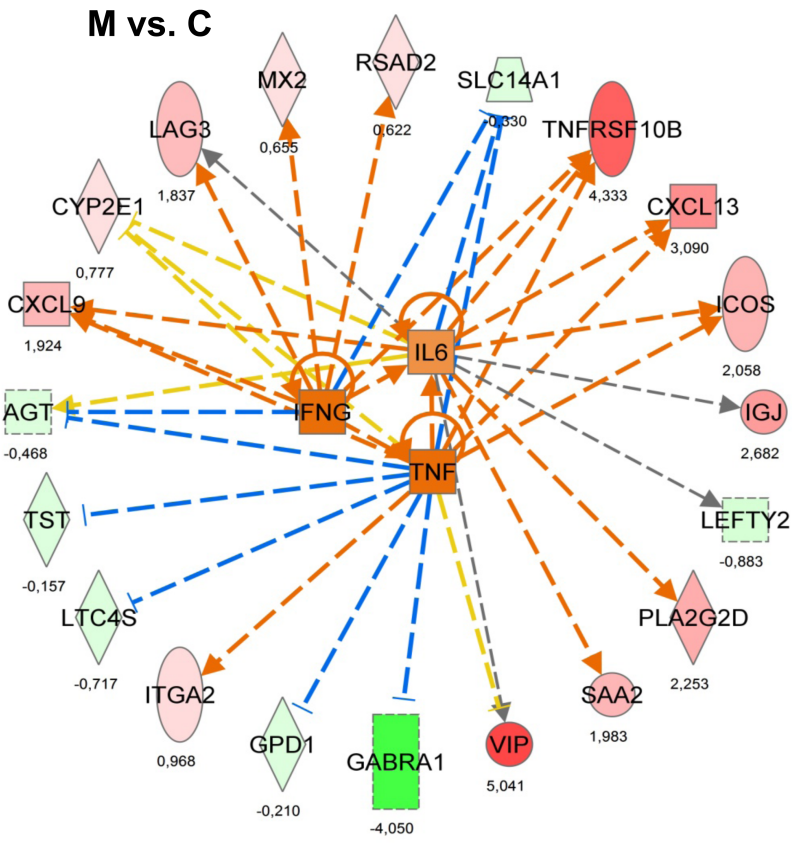
M vs. C
MX2
0,655
RSAD2
0,622
SLC14A1
0,330
LAG3
1,837
TNFRSF10B
4,333
CYP2E1
0,777
CXCL13
3,090
CXCL9
1,924
ICOS
2,058
IL6
IFNG
AGT
-0,468
IGJ
2,682
TNF
TST
-0,157
LEFTY2
-0,883
LTC4S
-0,717
PLA2G2D
2,253
ITGA2
0,968
SAA2
1,983
GPD1
-0,210
GABRA1
-4,050
VIP
5,041